CHEMISTRY
A EUROPEAN JOURNAL

FULL PAPER

DOI: 10.1002/chem.201301464

Heteroleptic Alkyl and Amide Iminoanilide Alkaline Earth and Divalent Rare Earth Complexes for the Catalysis of Hydrophosphination and (Cyclo)Hydroamination Reactions

Bo Liu,[a] Thierry Roisnel,[b] Jean-François Carpentier,*[a] and Yann Sarazin*[a]

Abstract: [{N^N}M(X)(thf)$_n$] alkyl (X = CH(SiMe$_3$)$_2$) and amide (X = N(SiMe$_3$)$_2$) complexes of alkaline earths (M = Ca, Sr, Ba) and divalent rare earths (Yb^{II} and Eu^{II}) bearing an iminoanilide ligand ({N^N}$^-$) are presented. Remarkably, these complexes proved to be kinetically stable in solution. X-ray diffraction studies allowed us to establish size–structure trends. Except for one case of oxidation with [{N^N}Yb^{II}{N(SiMe$_3$)$_2$}(thf)], all these complexes are stable under the catalytic conditions and constitute effective precatalysts for the cyclohydroamination of terminal aminoalkenes and the intermolecular hydroamination and intermolecular hydrophosphination of activated alkenes. Metals with equal sizes across alkaline earth and rare earth families display almost identical apparent catalytic activity and selectivity. Hydrocarbyl complexes are much better catalyst precursors than their amido analogues. In the case of cyclohydroamination, the apparent activity decreases with metal size: Ca > Sr > Ba, and the kinetic rate law agrees with $R_{CHA} = k$[precatalyst]^1[aminoalkene]^1. The intermolecular hydroamination and hydrophosphination of styrene are anti-Markovnikov regiospecific. In both cases, the apparent activity increases with the ionic radius (Ca < Sr < Ba) but the rate laws are different, and obey $R_{HA} = k$[styrene]^1[amine]^1[precatalyst]^1 and $R_{HP} = k$[styrene]^1[HPPh$_2$]^0[precatalyst]^1, respectively. Mechanisms compatible with the rate laws and kinetic isotopic effects are proposed. [{N^N}Ba{N(SiMe$_3$)$_2$}(thf)$_2$] (**3**) and [{N^N}Ba{CH(SiMe$_3$)$_2$}(thf)$_2$] (**10**) are the first efficient Ba-based precatalysts for intermolecular hydroamination and hydrophosphination, and display activity values that are above those reported so far. The potential of the precatalysts for C–N and C–P bond formation is detailed and a rare cyclohydroamination–intermolecular hydroamination "domino" sequence is presented.

Keywords: alkaline earth metals · hydroamination reactions · hydrophosphination reactions · rare earths · reaction mechanisms

Introduction

Catalyzed alkene hydrofunctionalizations consisting of the addition of H–X (X = Si, P, N, B…) bonds across C=C unsaturations represent a significant challenge the communities of organometallic and organic chemists are faced with.[1] Hydrophosphination (X = P) and even more so hydroamination (X = N) reactions have been at the center of attention in recent years, not least because the resulting phosphines and amines constitute valuable chemicals for a virtually boundless array of applications. Both can to some extent be catalyzed by late transition-metal (TM) catalysts that display characteristic robustness and functional-group tolerance, but suffer from limited lifetime, low reaction rates, and limited scope.[1,2] Hence, since the seminal breakthroughs,[3] left main group, early TM, and especially rare earth (RE) complexes have been at the forefront of catalyst development in this area.[2a,b,4] This is particularly true of hydrophosphination reactions, which, owing to the soft nature of the phosphorus atom, are much more efficiently catalyzed by complexes based on hard, highly Lewis acidic metals (Groups 3 and 4) than by soft, late TM-based catalysts.[2d,5–7]

Through a range of landmark contributions, Marks et al. demonstrated the potential of lanthanidocene catalysts in cyclohydrophosphination[7] and even more so hydroamination[3,8,9] reactions, and his work inspired that of many others.[10] Prompted by these results and by the similarities in the properties and reactivity of rare earth and alkaline earth (Ae) metals, Hill et al. implemented complexes of the large Ae metals (Sr, Ba but preponderantly Ca) as worthy precatalysts for the cyclohydroamination of aminoalkenes,[11] intermolecular alkene hydroamination,[12] and hydrophosphination[13] reactions, or a variety of other organic transforma-

[a] Dr. B. Liu, Prof. Dr. J.-F. Carpentier, Dr. Y. Sarazin
Organometallics: Materials and Catalysis
Institut des Sciences Chimiques de Rennes
UMR 6226 CNRS—Université de Rennes 1
Campus de Beaulieu, 35042 Rennes Cedex (France)
Fax: (+33) 223-236-939
E-mail: jean-francois.carpentier@univ-rennes1.fr
yann.sarazin@univ-rennes1.fr

[b] Dr. T. Roisnel
Centre de Diffractométrie X
Institut des Sciences Chimiques de Rennes
UMR 6226 CNRS—Université de Rennes 1
Campus de Beaulieu, 35042 Rennes Cedex (France)

Supporting information for this article is available on the WWW under http://dx.doi.org/10.1002/chem.201301464.

tions.[14] These precatalysts, and amongst them most prominently the versatile β-diketiminate calcium complex [{BDI}Ca{N(SiMe$_3$)$_2$}(thf)] ({BDI}H = H$_2$C{C(Me)N-2,6-(*i*Pr)$_2$C$_6$H$_3$}$_2$),[15] generally featured excellent performance. Several groups have since endeavored to develop original Ca-based catalysts for the cyclohydroamination of aminoalkenes[16] (some of which displayed appreciable levels of enantioselectivity)[16c,e–g] and hydrophosphination[17] of activated alkenes.[18,19] On the other hand, the use of Sr and Ba precatalysts remained underexplored, because the synthesis of stable heteroleptic complexes of the type [{L}AeX(solvent)$_n$] (where Ae is Sr or Ba, {L}$^-$ is a monoanionic ancillary ligand and X$^-$ is a reactive group, typically an amide) is hampered by their kinetic lability, which leads to facile decomposition in solution through deleterious Schlenk-type equilibria. Recently, we introduced several complete families of stable Ae heteroleptic complexes [{L}Ae(NR$_2$)(thf)$_n$] (Ae = Mg, Ca, Sr or Ba; {L}$^-$ = β-diketiminate, iminoanilide or aminophenolate; R = SiMe$_3$ or SiMe$_2$H; n = 0–2), which catalyzed both the intermolecular hydrophosphination and hydroamination of activated alkenes.[20] Surprisingly, the catalytic activity increased with the size of the metal, that is, (Mg ≪) Ca < Sr < Ba; in the case of Ba, intermolecular hydroamination reaction followed the empirical rate law given in Equation (1).

$$R_{HA} = k[\text{alkene}]^1[\text{amine}]^1[\text{Ba}]^1 \quad (1)$$

Yet, reaction rates in the cyclohydroamination of aminoalkenes catalyzed by the same β-diketiminate or aminophenolate Ae complexes decreased in the order Ca > Sr > Ba,[21] as reported by Hill et al.[11]

The divalent rare earth metals (RE^{II}) Yb^{II} and Eu^{II} display almost identical ionic radii to Ca and Sr, respectively (ionic radii for C.N. = 6: Ca, 1.00 Å; Sr, 1.18 Å; Yb^{II}, 1.02 Å; Eu^{II}, 1.17 Å),[22] and also feature many close properties. All are hard, electropositive elements, forming d^0 complexes where non-directional bonding is prominently governed by electrostatic and steric interactions. Comparative studies between the catalytic behavior of congeneric families of Ae and RE^{II} catalysts remain scarce, but partial (Eu^{II}, 4f^7) or complete (Yb^{II}, 4f^{14}) filling of low-lying f orbitals with their limited radial extension and the redox-active nature of RE^{II} elements have not been shown to systematically induce different reactivity between related RE^{II} and Ae complexes.[17,23] An example pertaining to the present study was disclosed in 2012 by Cui et al.,[17] with heteroleptic Ca and Yb^{II} catalysts containing a tridentate iminoamidinate ligand: commensurate activity but different selectivity were observed in the hydrophosphination of alkynes; yet, both Ca and Yb^{II} afforded very similar results in the hydrophosphination of dienes. Just as in Takaki's hydrophosphination of alkynes promoted by organoytterbium complexes,[24] no change of the oxidation state of the (Yb^{II}) metal center was detected.

Building on an earlier communication,[20] we now report the synthesis and structural characterization of stable heteroleptic complexes [{N^N}M(X)(thf)$_n$] (M = Ca, Sr, Ba, Yb^{II}, Eu^{II}) supported by an iminoanilide ancillary ligand ({N^N}$^-$)[25] and incorporating an amide (X$^-$ = N(SiMe$_3$)$_2^-$) or alkyl (X$^-$ = CH(SiMe$_3$)$_2^-$) reactive group, and their ability to catalyze the hydrophosphination and (cyclo)hydroamination of alkenes. The competences of the respective families are detailed and relevant kinetic parameters and plausible mechanistic scenarios are presented.

Results and Discussion

Synthesis and characterization: In a similar fashion to that described for the previously reported [{N^N}Ae{N(SiMe$_3$)$_2$}(thf)$_x$] (Ae = Ca, x = 1, **1**; Sr, x = 2, **2**; Ba, x = 2, **3**),[20] the two divalent rare earth complexes [{N^N}RE^{II}{N(SiMe$_3$)$_2$}(thf)$_x$] (RE^{II} = Yb^{II}, **4**, x = 1; Eu^{II}, **5**, x = 2) were obtained in good yields (ca. 60–70%) upon one-pot reaction of the iminoaniline proteo-ligand {N^N}H and [RE^{II}I$_2$(thf)$_2$] with 2 equivalents of KN(SiMe$_3$)$_2$ (Scheme 1).

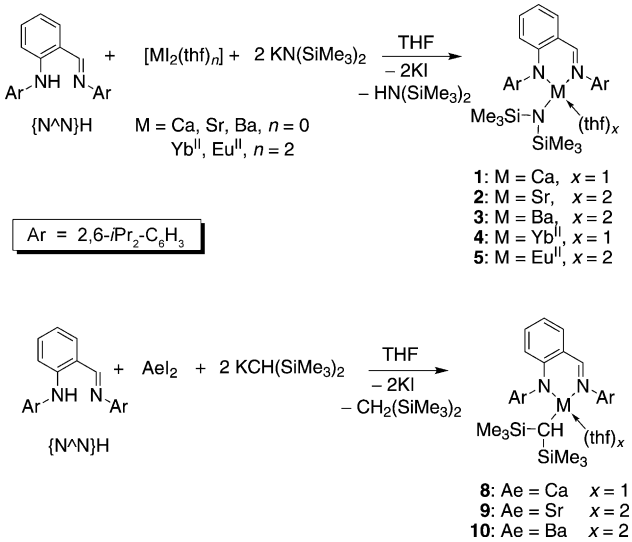

Scheme 1.

The identity of **4** and **5** (isolated as dark purple and dark red powders, respectively) was established by X-ray diffraction crystallography, and their purity was confirmed by combustion analysis. The diamagnetic **4** was also characterized by conventional NMR techniques which attested to the stability of the complex in solution (no sign of decomposition was observed in C$_6$D$_6$ solutions after 3 days at room temperature), but the strongly paramagnetic nature of the Eu^{II} complex **5** precluded acquisition of informative NMR data. Both complexes are highly air- and moisture-sensitive, and this thwarted all attempts to obtain mass spectrometry data. The iminoanilide Ca and Yb^{II} complexes **1** and **4** can be seen as the direct analogues, yet with a more rigid ligand framework, to the β-diketiminate complexes [{BDI}Ca{N(SiMe$_3$)$_2$}(thf)] (**6**) and [{BDI}Yb^{II}{N(SiMe$_3$)$_2$}(thf)] (**7**) that

have been reported elsewhere.[11a,15,26] Attempts to prepare the samarium congener of complexes **4** and **5** were inconclusive, as the only product which could be characterized beyond doubt was the bis(iminoanilide) complex $[\{N\hat{}N\}_2Sm^{II}(thf)]$;[27,28] apparently, the targeted heteroleptic Sm^{II} complex suffered from kinetic lability, but whether $[\{N\hat{}N\}_2Sm^{II}(thf)]$ was the main product of this reaction or simply a minor by-product could not be ascertained.

The one-pot reaction of $KCH(SiMe_3)_2$, {N^N}H and AeI_2 in a 2:1:1 ratio afforded the stable heteroleptic Ae-alkyls complexes $[\{N\hat{}N\}Ae\{CH(SiMe_3)_2\}(thf)_x]$ (Ae = Ca, $x=1$, **8**; Sr, $x=2$, **9**; Ba, $x=2$, **10**) in 50–70% yield as yellow solids (Scheme 1). Their identity was determined by NMR spectroscopy, and was corroborated by elemental analysis and, for **9** and **10**, by X-ray diffraction crystallography. All are fully soluble and stable in aromatic solvents, as indicated by ^1H NMR monitoring in C_6D_6 solution at 25–60 °C, and they can also be dissolved in aliphatic hydrocarbons. If a few heteroleptic Ca complexes of the type $[\{L\}CaR(solvent)_n]$ bearing a multidentate monoanionic ligand ($\{L\}^-$) and a hydrocarbyl group (R^-) have already been authenticated by X-ray diffraction methods,[29] to our knowledge analogous heteroleptic Sr- and Ba-alkyl complexes have only been generated in situ or characterized by NMR spectroscopy.[11f,29c,30] Complexes **9** and **10** hence represent the first heteroleptic Sr- and Ba-alkyl species structurally characterized. Much as found for their amido derivatives **2** and **3**,[20] their kinetic stability can be attributed to the steric shielding conferred to the metal center by the very hindered $\{N\hat{}N\}^-$ ancillary (see below); besides, by opposition to $\{BDI\}^-$ or bis(imino)acenapthene ligands which respectively undergo deprotonation[29c] or dearomatization[11f] in the presence of basic $Ae^{\delta+}\cdots^{\delta-}CH(SiMe_3)_2$ moieties for Ae = Sr or Ba, we found that the $\{N\hat{}N\}^-$ ligand framework was chemically inert towards $CH(SiMe_3)_2^-$ in the three complexes **8**–**10**.[31]

The crystal structures of several of these complexes were determined, and relevant metric parameters are collected in Table 1.

Unusually for the large Sr element,[32] the metal center in $[\{N\hat{}N\}Sr\{N(SiMe_3)_2\}(thf)]$ (**2′**) is only 4-coordinate in **2′** (Figure 1). The tetrahedral arrangement in **2′** is less distorted than in equally 4-coordinate $[\{BDI\}Sr\{N(SiMe_3)_2\}(thf)]$,[33] even if the related bond lengths in the two complexes all fall within the same range.

The Yb^{II} complex **4** is also 4-coordinate and rests in a distorted tetrahedral geometry, approaching trigonal monopyramidal (Figure 2). The Yb^{II}-heteroatom bond lengths in **4** are shorter than in **2′**, as expected on account of the smaller ionic radius of Yb^{II} (1.02 Å) versus that of Sr (1.18 Å).

The Eu^{II} complex **5** features the metal center in a slightly distorted square pyramidal geometry ($\tau=0.13$),[34] with the amide (N41) in apical position (Figure 3). The Eu1–$N4_{anilidino}$ bond length of 2.53 Å is substantially shorter than that between the metal center and $N25_{imino}$ (2.66 Å), an evidence for the limited degree of delocalization of the negative charge in the N4-C3-C23-C24-N25 backbone. By comparison, the two Eu^{II}–N_{ATI} distances are almost identical (2.54 and 2.56 Å) in Roesky's aminotroponiminate ($\{ATI\}^-$) $[\{ATI\}Eu^{II}\{N(SiMe_3)_2\}(thf)_2]$.[16b] The Eu^{II}–N_{BDI} bond lengths in Shen's 5-coordinate $[\{BDI\}_2Eu^{II}(thf)]$, where the charge is

Table 1. Structural parameters for $[\{L\}M(X)(solvent)_x]$ complexes (M = Ca, Sr, Ba, Yb^{II}, Eu^{II}; $X^- = N(SiMe_3)_2^-$, $N(SiMe_2H)_2^-$, $CH(SiMe_3)_2^-$) bearing nitrogen-based $\{L\}^-$ bidentate ligands.

Entry	Complex		r_{ionic} [Å][a]	CN[b]	M–X [Å][c]	N-M-N [°][d]	M···NCCCN [Å][e]	Ref.
1	$[\{N\hat{}N\}Ca(N(SiMe_3)_2)(thf)]$	**1**	1.00	4	2.29	77.4	0.81	[20]
2	$[\{N\hat{}N\}Sr(N(SiMe_3)_2)(thf)]$	**2′**	1.18	4	2.46	71.3	0.68	this work
3	$[\{N\hat{}N\}Ba(N(SiMe_3)_2)(thf)_2]$	**3**	1.35	5	2.62	66.0	1.14	[20]
4	$[\{N\hat{}N\}Yb^{II}(N(SiMe_3)_2)(thf)]$	**4**	1.02	4	2.34	76.6	1.12	this work
5	$[\{N\hat{}N\}Eu^{II}(N(SiMe_3)_2)(thf)_2]$	**5**	1.17	5	2.48	71.0	0.97	this work
6	$[\{BDI\}Ca(N(SiMe_3)_2)(thf)]$	**6**	1.00	4	2.31	81.1	1.22	[15]
7	$[\{BDI\}Yb^{II}(N(SiMe_3)_2)(thf)]$	**7**	1.02	4	2.34	82.1	1.61	this work
8	$[\{BDI\}Sr(N(SiMe_3)_2)(thf)]$	**11**	1.18	4	2.45	74.1	0.72	[33]
9	$[\{BDI\}Ba(N(SiMe_3)_2)(thf)]$	**12**	1.35	4	2.59	69.7	1.88	[39]
10	$[\{BDI\}Ca(N(SiMe_2H)_2)(thf)]$	**13**	1.00	4	2.31	80.9	0.82	[20]
11	$[\{BDI\}Sr(N(SiMe_2H)_2)(thf)_2]$	**14**	1.18	5	2.47	74.7	1.31	[21]
12	$[\{BDI\}Ba(N(SiMe_2H)_2)(thf)_2]$	**15**	1.35	5	2.61	68.8	1.45	[20]
13	$[\{N\hat{}N\}Sr(CH(SiMe_3)_2)(thf)_2]$	**9**·C_5H_{12}	1.18	5	2.71	71.3	1.09	this work
14	$[\{N\hat{}N\}Ba(CH(SiMe_3)_2)(thf)_2]$	**10**	1.35	5	2.84	66.3	1.18	this work

[a] Ionic radius of the metal (M) for CN = 6. [b] CN = Coordination number of the metal in the complex. [c] Distance between metal center and alkyl/amide reactive group. [d] Bite angle formed through bidentate chelation of the ancillary ligand. [e] Distance between metal center and mean plane defined by the $N_{ancillary}$-C-C-C-$N_{ancillary}$ backbone in the ancillary ligand.

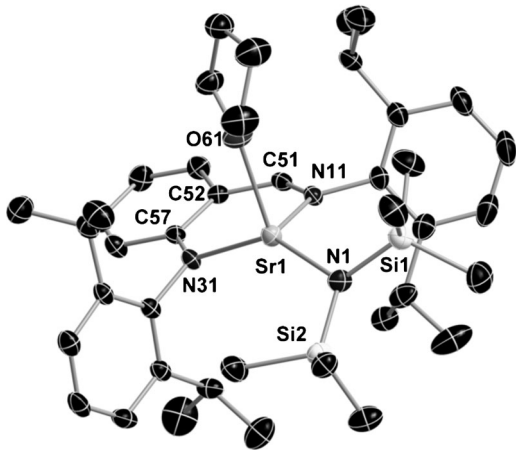

Figure 1. X-ray structure of $[\{N\hat{}N\}Sr\{N(SiMe_3)_2\}(thf)]$ (**2′**). Ellipsoids are drawn at the 50% probability level. Hydrogen atoms are omitted for clarity. Selected bond lengths (Å) and angles (°): Sr1–N1 2.463(2), Sr1–O61 2.491(2), Sr1–N31 2.512(2), Sr1–N11 2.574(2), Si1–N1 1.692(2), Si2–N1 1.688(2); N1-Sr1-O61 101.09(6), N1-Sr1-N31 145.27(6), O61-Sr1-N31 106.51(6), N1-Sr1-N11 123.18(6), O61-Sr1-N11 101.63(6), N31-Sr1-N11 71.32(5), Si2-N1-Si1 126.1(1), Si2-N1-Sr1 115.18(9), Si1-N1-Sr1 118.7(1).

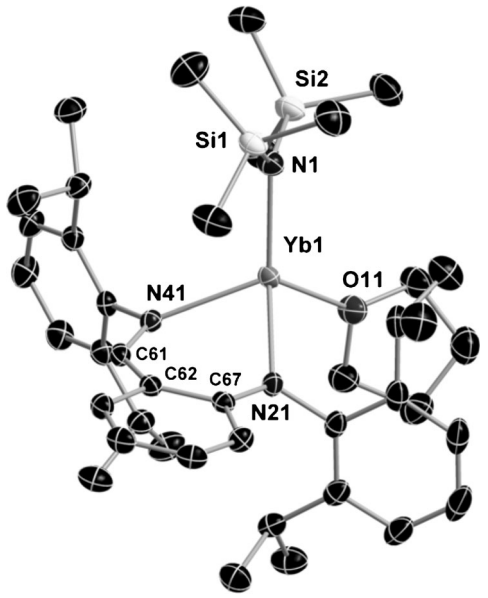

Figure 2. X-ray structure of [{N^N}Yb^{II}{N(SiMe$_3$)$_2$}(thf)] (**4**). Ellipsoids are drawn at the 50% probability level. Hydrogen atoms are omitted for clarity. Selected bond lengths (Å) and angles (°): Yb1–N1 2.339(2), Yb1–N21 2.375(2), Yb1–O11 2.395(1), Yb1–N41 2.412(2); N1-Yb1-N21 127.82(5), N1-Yb1-O11 119.16(5), N21-Yb1-O11 96.51(5), N1-Yb1-N41 111.14(5), N21-Yb1-N41 76.60(5), O11-Yb1-N41 118.97(5).

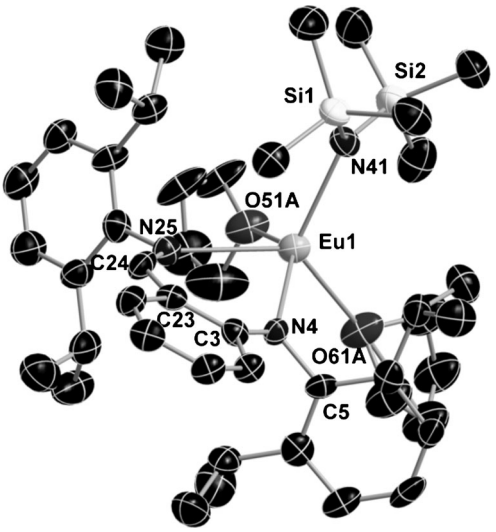

Figure 3. X-ray structure of [{N^N}Eu^{II}{N(SiMe$_3$)$_2$}(thf)$_2$] (**5**). Ellipsoids are drawn at the 50% probability level. Hydrogen atoms are omitted for clarity. Only the mains components of the disordered coordinated THF molecules are represented. Selected bond lengths (Å) and angles (°): Eu1–N41 2.483(8), Eu1–N4 2.529(7), Eu1–O51A 2.600(7), Eu1–N25 2.656(7), Eu1–O61A 2.689(7); N41-Eu1-N4 115.6(2), N41-Eu1-O51A 105.4(2), N4-Eu1-O51A 136.6(2), N41-Eu1-N25 110.7(2), N4-Eu1-N25 71.0(2), O51A-Eu1-N25 81.9(2), N41-Eu1-O61A 119.3(3), N4-Eu1-O61A 96.0(2), O51A-Eu1-O61A 74.9(2), N25-Eu1-O61A 128.7(2).

fully delocalized over the N_{BDI}-C-C-C-N_{BDI} core, fall in the range 2.53–2.59 Å.[35]

The structure of the known β-diketiminate complex [{BDI}Yb^{II}{N(SiMe$_3$)$_2$}(thf)] (**7**)[26] is discussed here for the first time (Figure 4). The metal center in **7** is 4-coordinate and much as in **4**, it exists in a highly distorted, almost trigonal monopyramidal, environment. Significant discrepancies between the arrangement in the two complexes include the distance from Yb^{II} to the N1-C2-C3-C4-N5 mean plane (1.61 Å in **7**, and "only" 1.12 Å in **4**, see above) and a wider $N_{ancillary}$-Yb^{II}-$N_{ancillary}$ bite angle for the β-diketiminate complex (76.6° in **4** versus 82.1° in **7**).

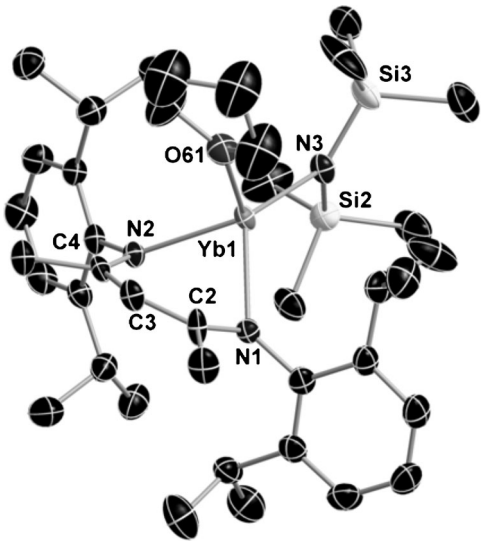

Figure 4. X-ray structure of [{BDI}Yb^{II}{N(SiMe$_3$)$_2$}(thf)] (**7**). Ellipsoids are drawn at the 50% probability level. Hydrogen atoms are omitted for clarity. Selected bond lengths (Å) and angles (°): Yb1–N3 2.341(3), Yb1–N2 2.363(3), Yb1–N1 2.379(3), Yb1–O61 2.424(3); N3-Yb1-N2 120.3(1), N3-Yb1-N1 127.8(1), N2-Yb1-N1 82.1(1), N3-Yb1-O61 115.6(1), N2-Yb1-O61 104.3(1), N1-Yb1-O61 100.5(1).

The 5-coordinate Sr atom in [{N^N}Sr{CH(SiMe$_3$)$_2$}-(thf)$_2$]·C$_5$H$_{12}$ (**9**·C$_5$H$_{12}$) exits in a near-perfect square pyramidal environment ($\tau = 0.06$),[34] with the bulky CH(SiMe$_3$)$_2^-$ group located on the apex (Figure 5). The Sr1–N31 bond length (2.52 Å) is noticeably shorter than the Sr1–N11 one (2.63 Å), again highlighting the limited delocalization on the negative charge over the N11-C24-C25-C30-N31 backbone. The long Sr1–C1 distance (2.71 Å) in **9**·C$_5$H$_{12}$ suggests that this $^{\delta+}$Sr–C$_{alkyl}^{\delta-}$ bond is highly ionic, but it matches that found in related organometallic Sr complexes exhibiting σ-bound alkyl groups;[36] amongst these, **9**·C$_5$H$_{12}$ stands out as being the only heteroleptic mononuclear alkyl complex of the type [{L}SrR(solvent)$_n$].

The arrangement about Ba in [{N^N}Ba{CH(SiMe$_3$)$_2$}-(thf)$_2$] (**10**) resembles that in the Sr analogue **9**·C$_5$H$_{12}$ (Figure 6). The 5-coordinate metal center sits in a square pyramidal geometry ($\tau = 0.06$),[34] with the apical position occupied by CH(SiMe$_3$)$_2^-$. The N141-Ba2-N111 bite angle of 66.3° is narrow, and the distance from the very large Ba atom to the mean plane delineated by N141-C142-C147-C148-N111 is 1.18 Å; both values match those found in the amido derivative **3** (66.0° and 1.14 Å respectively).[20] Barium compounds featuring Ba–C σ bonds are not exceptional,[36,37] but to our knowledge **10** represents the first ex-

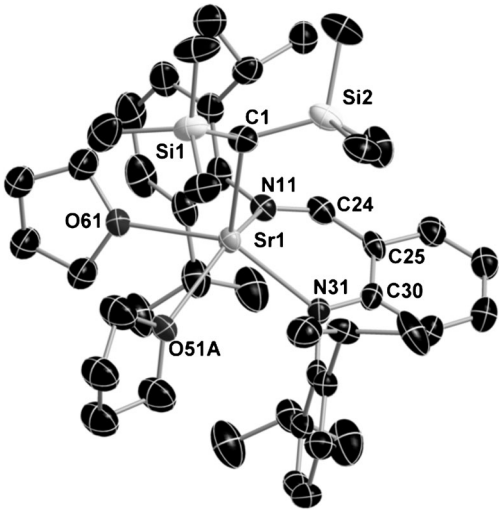

Figure 5. X-ray structure of $[\{N\hat{}N\}Sr\{CH(SiMe_3)_2\}(thf)_2]\cdot C_5H_{12}$ (**9**·C_5H_{12}). Ellipsoids are drawn at the 50% probability level. Hydrogen atoms and the non-interacting pentane molecule are omitted for clarity. Only the main component of the disordered coordinated THF molecule (namely O51A) is represented. Selected bond lengths (Å) and angles (°): Sr1–N31 2.524(3), Sr1–O61 2.528(3), Sr1–O51A 2.570(3), Sr1–N11 2.627(3), Sr1–C1 2.706(4); N31-Sr1-O61 133.5(1), N31-Sr1-O51A 95.6(1), O61-Sr1-O51A 75.16(9), N31-Sr1-N11 71.3(1), O61-Sr1-N11 84.9(1), O51A-Sr1-N11 137.1(1), N31-Sr1-C1 124.6(1), O61-Sr1-C1 100.5(1), O51A-Sr1-C1 111.7(1), N11-Sr1-C1 109.1(1).

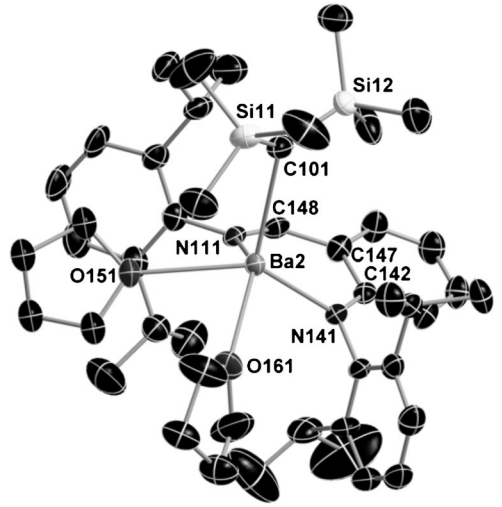

Figure 6. X-ray structure of $[\{N\hat{}N\}Ba\{CH(SiMe_3)_2\}(thf)_2]$ (**10**). Ellipsoids are drawn at the 50% probability level. Hydrogen atoms omitted for clarity. Only one of the two independent molecules is depicted, and only the main component of the disordered coordinated THF molecule (namely O151) is shown. Selected bond lengths (Å) and angles (°): Ba2–N141 2.652(6), Ba2–O151 2.741(5), Ba2–O161 2.782(5), Ba2–N111 2.815(6), Ba2–C101 2.840(7); N141-Ba2-O151 131.2(2), N141-Ba2-O161 99.8(2), O151-Ba2-O161 73.8(2), N141-Ba2-N111 66.3(2), O151-Ba2-N111 83.4(2), O161-Ba2-N111 133.6(2), N141-Ba2-C101 118.5(2), O151-Ba2-C101 104.0(2), O161-Ba2-C101 122.6(2), N111-Ba2-C101 101.7(2).

ample of an heteroleptic Ba-alkyl complex that has been structurally authenticated.[38] The Ba2–C101 bond length of 2.84 Å is typical of alkyl or alkyne groups σ-bonded to Ba.[36]

Pertinent structural data for the families of Ae and RE^{II} complexes supported by the isoelectronic N,N-bidentate ligands $\{N\hat{}N\}^-$ (**1**–**5** and **9**–**10**) and $\{BDI\}^-$ (**6**,**7**, **11**–**15**) are displayed in Table 1. Several features emerge from the comparison of the structural data for **1**–**15**. The N-M-N bite angle depends largely on the ionic radius of the element: irrelevantly of the coordination number of the metal in a given family of complexes (i.e. β-diketiminate or iminoanilide), the bite angle decreases with increasing metal size (Table 1, entries 1–6 and 8–14), but remains constant for metals of identical ionic radii (compare entries 1 and 4, 2 and 5, 6 and 7). Besides, the bite angle shows no dependence upon the identity of the reactive group ($N(SiMe_3)_2^-$, $N(SiMe_2H)_2^-$, or $CH(SiMe_3)_2^-$) attached to the metal, compare entries 6 and 10, 8 and 11, 9 and 12, 2 and 13, or 3 and 14. If the very large Ba atom is essentially 5-coordinate in these complexes, coordination of 4 atoms is sufficient to meet the stereoelectronic requirements for the smaller Ca and Yb^{II} metals. No obvious pattern emerges in the case of strontium, which features intermediate size between Ca and Ba. It is unclear why the M···N-C-C-C-N distance in complexes **6** (1.22 Å) and **7** (1.61 Å) exhibit such a difference when all other metric parameters between the two complexes remain commensurate.[40] Similar observations are made between **1** and **4**, as well as between **2** and **5**, even if the coordination differs in these last two complexes. Discrepancies in the location of the metal center are observed in related Ca, Sr, and Ba complexes (e.g., **6**, **11**, and **12**). The important role of d orbitals (with 4d orbitals in Sr being energetically more accessible than 3d orbitals in Ca) in the bonding pattern in neutral and cationic β-diketiminate complexes of Ca and Sr has been highlighted,[41] and was shown to be a decisive factor in the relative position of the metal vis-à-vis the N_{BDI}-C-C-C-N_{BDI} average plane; these considerations may explain the peculiar position of the Ba atom in Hill's complex **12**.[39] The nature and overall steric bulk of the amido group ($X^- = N(SiMe_3)_2^-$ or $N(SiMe_2H)_2^-$) is found to play no part in the pertaining Ae–N_{amide} bond lengths even for complexes where the coordination number of the metal varies (compare entries 6 and 10, 8 and 11, 9 and 12). Yet, the Ba–C_{alkyl} bond length in **10** (entry 14, 2.84 Å) is much greater than the related Ba–N_{amide} one in **3** (entry 3, 2.62 Å).

Catalysis of hydroelementation reactions: The performance of heteroleptic complexes **1**–**5** and **8**–**10** incorporating the $\{N\hat{}N\}^-$ ligand as catalysts in the cyclohydroamination of aminoalkenes, intermolecular hydroamination and hydrophosphination of activated alkenes were interrogated (Figure 7). The aptitude of complexes supported by the β-diketiminate ligand $\{BDI\}^-$ was reported elsewhere,[20,21] and the Ca and Yb^{II} complexes **6** and **7** are therefore only included for comparative purposes.

Cyclohydroamination reactions: The ability of **1**–**10** to catalyze cyclohydroamination reactions was probed by examining their performance in the cyclization of 1-amino-2,2-di-

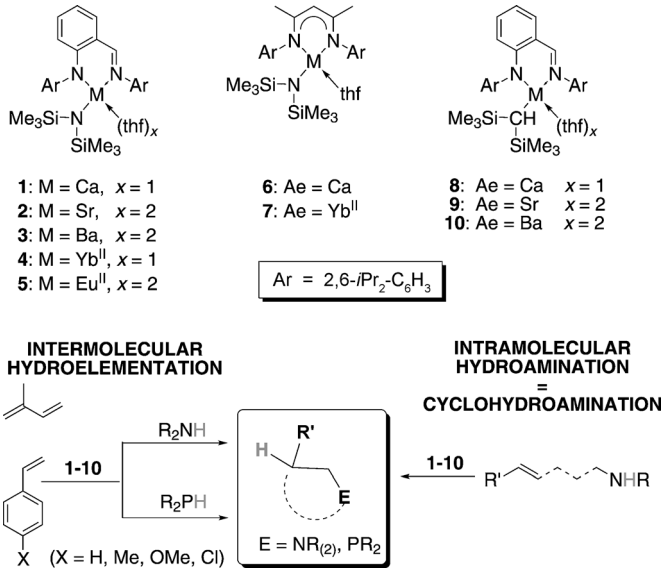

Figure 7. (Cyclo)hydroelementation reactions catalyzed by complexes **1**–**10**.

Table 2. Representative data for the cyclohydroamination of **S** catalyzed by **1**–**10**.

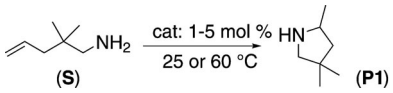

(**S**) (**P1**)

Entry	Precatalyst	Reaction conditions[a]	time [min]	Conversion [%][b]	k_{app} [10^{-4} s^{-1}][c]
1	**1**	A	4	90	120
2	**2**	B	7	97	68
3	**3**	B	60	96	6
4	**4**	A	4	96	140
5	**5**	B	7	98[d]	nd[e]
6	**6**	A	4	27	15
7	**7**	A	4	29	16
8	**8**	A	<2	100	nd[f]
9	**9**	A	<3	98	nd[f]
10	**10**	A	20	96	22
11	**10**	C	5	97	101

[a] Reaction conditions A: [precat]/[**S**] = 1:100, precat: 5.0 μmol, C_6D_6: 1.2 mL, 25 °C; Reaction conditions B: [precat]/[**S**] = 1:50, precat: 10.0 μmol, C_6D_6: 0.6 mL, 60 °C; Reaction conditions C: [**10**]:[**S**] = 1:50, precat: 10.0 μmol, C_6D_6: 0.6 mL, 25 °C. [b] Conversion determined by ^{1}H NMR spectroscopy. [c] Determined by ^{1}H NMR monitoring experiments. [d] Determined after quenching of the reaction and removal of paramagnetic Eu^{II} species. [e] NMR measurements precluded by the paramagnetic nature of the complex. [f] Reaction too fast to allow accurate NMR kinetic monitoring.

methyl-4-pentene (**S**), a common aminoalkene for which abundant data is available in the literature. Representative results are given in Table 2. Ring-closure of 50–100 equivalents of substrate proceeded at 25–60 °C according to Baldwin's guideline (5-*exo*-trig) in all cases, leading to the exclusive formation of 2,4,4-trimethylpyrrolidine (**P1**).

Several trends appear upon examination of these qualitative results. First, the apparent catalytic activity increases with decreasing ionic radius (compare entries 1–3, 4–5 or 8–10 in Table 2), and therefore Ca (and Yb^{II}) provided the most efficient precatalysts for the cyclohydroamination of alkenes, whereas Ba ones were the least efficient. This is in agreement with earlier reports by several groups;[11,16b,21] however, this trend is reversed during intermolecular reactions (see below). Secondly, metals with similar ionic radii across Ae and RE^{II} families exhibit essentially identical catalytic activity (compare entries 1 and 4, 6 and 7, or 2 and 5). No sign of oxidation of the RE^{II}-based catalysts **4** and **5** was detected under catalytic conditions, since the color of the solution remained the same throughout the whole duration of the catalyzed reactions (purple for **4** and dark red for **5**), and reactions involving the diamagnetic **4** could be adequately monitored by ^{1}H NMR spectroscopy until completion. This contrasts with tidings from Roesky et al., who found that [{ATI}Yb^{II}{$N(SiMe_3)_2$}(thf)$_2$] was catalytically competent (albeit generally less so than its direct Ca analogue), but was very rapidly oxidized under the chosen conditions;[16b] the bis(phosphinimino)methanide complex [{$(Me_3SiNPPh_2)_2CH$}YbI(thf)$_2$] also oxidized during the cyclohydroamination of aminoalkenes and aminoalkynes.[23b] Hence, the {N^N}$^-$ iminoanilide appears as a valuable ancillary to stabilize these reactive redox centers. Moreover, for a given metal, the {N^N}$^-$ iminoanilide displays markedly higher performance than the β-diketiminate scaffold, compare for instance entries 1 and 6 (for Ca) or entries 4 and 7 for Yb^{II}. Finally, complexes incorporating the highly reactive $CH(SiMe_3)_2^-$ alkyl group (as in **8**-**10**) are much more efficient than their derivatives bearing the $N(SiMe_3)_2^-$ group (as in **1**-**3**). This has also been seen by Hill et al.,[11 g] and can be explained in terms of relative acidity:[21,42] With a pK_a difference greater than 15 between $N(SiMe_3)_2^-$ and $CH(SiMe_3)_2^-$ in favor of the latter,[43] the more basic the reactive X^- group, the more easily the [M]–X bond reacts with the acidic aminoalkene to generate the catalytically active species [M]–$N(H)CH_2CMe_2CH_2CH{=}CH_2$ in the case of substrate **S** upon release of HX. The NMR spectra of in situ reactions catalyzed by **3** and **10** confirmed this interpretation: whereas the presence of free $HN(SiMe_3)_2$ could never be detected in the reaction catalyzed by **3** (as seen with other Ae catalysts),[11,21] quantitative release of $CH_2(SiMe_3)_2$ was observed in the case of **10**. These reactivity features are epitomized with [{N^N}Ca{$CH(SiMe_3)_2$}(thf)] (**8**), for which complete conversion of 100 equivalents of **S** is observed within 2 min at room temperature; **8** is to date the most effective Ae-based catalyst for the cyclohydroamination of the aminoalkene **S** (Table 2, entry 8), outperforming the ubiquitous **6**,[11a] homoleptic Ae complexes such as [Ae{$N(SiMe_3)_2$}$_2$(thf)$_x$] (x = 0 or 2) or [Ae{$CH(SiMe_3)_2$}$_2$(thf)$_2$],[11g] or heteroleptic aminophenolate-, bis(oxazoline)- or aminotroponiminate-based ones.[16,21]

Kinetic monitoring was performed by ^{1}H NMR spectroscopy to inform us on the behavior of these precatalysts. Complex **5**, which is paramagnetic, and complexes **8** and **9**, which are too fast for reliable measurements, were excluded from this set of experiments. The number of coordinated molecules of substrate could not be assessed. The fate of the

THF molecules during catalysis could not be established clearly because of partial overlap of resonances in the ^{1}H NMR spectra of in situ monitored reactions; yet, based on comparison the downfield resonances of free and coordinated THF in C_6D_6, it seemed that the solvent molecule(s) were released from the metal center under catalytic conditions. In all other cases, the monitoring indicated that substrate consumption followed first order kinetics in substrate concentration; no induction period was observed. The semi-logarithmic plots of monomer conversion versus reaction time are linear over 3 half-lives.[28] The values for the apparent rate constants (k_{app}, with $k_{app}=k[\mathbf{3}]^1$ expressed in s^{-1} and in which k is the reaction rate constant in $L\,mol^{-1}s^{-1}$, see below) extracted from these plots (Table 2) are in the range 0.0005–0.0020 s^{-1} for the less effective precatalysts to 0.012–0.014 s^{-1} for the most effective ones (**1** and **4**) that could be measured. They are consistent with the relationships previously discussed, that is, Ca > Sr > Ba, Ca ~ Yb^{II}, {N^N}$^-$ > {BDI}$^-$, and CH(SiMe$_3$)$_2^-$ ≫ N(SiMe$_3$)$_2^-$. First-order dependence upon substrate concentration was also measured for the complexes [{BDI}Ae{N(SiMe$_2$H)$_2$}(thf)$_2$] **13**–**15**,[21] but this contrasts with findings by others that the rate law for cyclohydroamination reactions catalyzed by trivalent rare earth systems is zeroth-order in [substrate].[3,8,10l] Other unusual behaviors have been mentioned before: Hill has reported that reaction rates were inversely proportional to substrate concentration in cyclohydroamination reactions catalyzed by **6** and its magnesium equivalent,[11d,g] whereas Hultzsch has described magnesium–phenolate precatalysts which exhibited either zeroth or second order decay in substrate concentration.[19e]

Competent barium precatalysts for hydroelementation reactions are seldom,[20,21] hence more attention was paid to **3** and **10**. The cyclohydroamination of **S** catalyzed by **3** at 60 °C was performed with $[\mathbf{3}]_0$ varying in a 12-fold range (3.80–46.3 mM). The linear plot of ln(k_{app}) versus ln($[\mathbf{3}]_0$) has a slope of 1.05 ($R^2=0.975$) indicating first-order dependence upon precatalyst concentration (Figure 8). Thus, the rate law for the cyclohydroamination of the aminoalkenes **S** catalyzed by **3** is given by Equation (2).

$$R_{CHA} = k[\mathbf{3}]^1[\text{aminoalkene}]^1 \quad (2)$$

The same rate law was also established for the Ba-alkyl precatalyst **10**.[28] Catalytic systems featuring such kinetic rate laws are uncommon;[42,44] to our knowledge there is no example with large Ae-based (Ca, Sr, or Ba) precatalysts. Relevant examples include Sadow's Mg complex supported by a tris(oxazolinyl)phenylborate ligand,[19f] and Hultzsch's phenoxyamine-Mg enantioselective precatalysts.[19h] Sadow proposed a convincing mechanism compatible with this rate law, whereby cyclization did not occur through migratory insertion of the polarized olefin into the Mg–N bond, as commonly proposed for zeroth order in [substrate], but rather through a six-centered concerted transition state (TS) mechanism involving transfer of a proton from a coordinated substrate molecule concomitant with ring-closure.[19f] It is plausible that such a mechanistic scenario is also at work in the case of **3**. A significant kinetic isotope effect ($k_{app}^{H_2}/k_{app}^{D_2}=2.60$; Figure 9) during the cyclohydroamination of **S** ($k_{app}^{H_2}=14.47(0.36)\times10^{-4}\,s^{-1}$) or its ND_2 deuterated analogue **S**-[$\mathbf{D_2}$] ($k_{app}^{D_2}=5.56(0.10)\times10^{-4}\,s^{-1}$) is consistent with this hypothesis.

The activation energy for **3** ($E_{a,\mathbf{3}}=98.2(4.5)\,kJ\,mol^{-1}$) and **10** ($E_{a,\mathbf{10}}=29.2(2.1)\,kJ\,mol^{-1}$) were determined from the Arrhenius plot of ln(k_{app}) versus 1/T in the temperature range 25–60 °C.[28] Although performed with a limited (4) set of

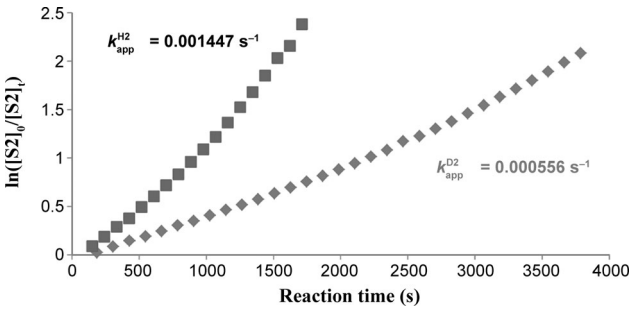

Figure 9. Kinetic isotopic measurements: Semi-logarithmic plot of substrate consumption versus time for the cyclohydroamination of **S** (■) and **S**-d_2 (◆) catalyzed in C_6D_6 (0.6 mL) at 60 °C by [{N^N}Ba{N(SiMe$_3$)$_2$}(thf)$_2$] (**3**), using 10.0 μmol of **3** and [substrate]$_0$/[**3**]$_0$ = 50:1.

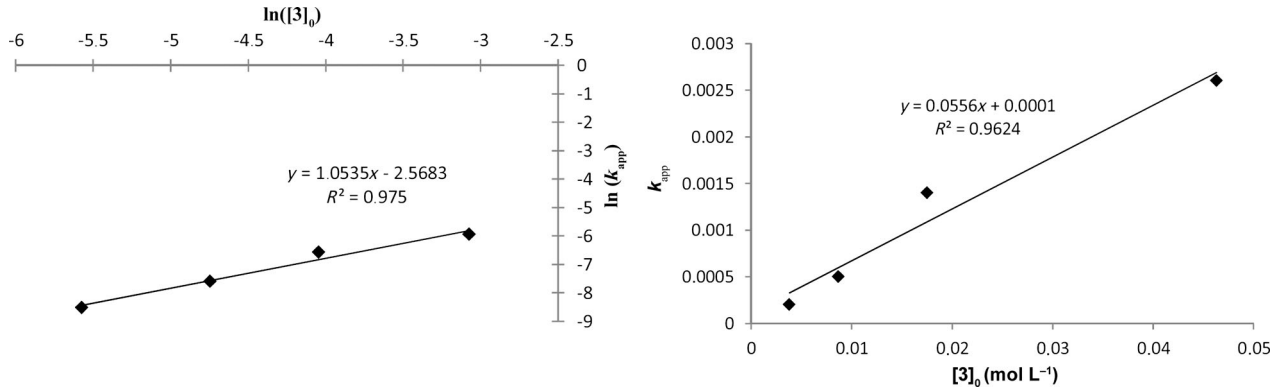

Figure 8. Plots of ln(k_{app}) versus ln($[\mathbf{3}]_0$) (left) and k_{app} versus $[\mathbf{3}]_0$ (right) for the cyclohydroamination of **S** catalyzed by [{N^N}Ba{N(SiMe$_3$)$_2$}(thf)$_2$] (**3**) at different precatalyst concentrations (3.8, 8.7, 17.5, and 46.3 mM). Reaction conditions: 60 °C, C_6D_6: 0.6 mL.

data points for practical reasons, the quality of the data for **3** and **10** was overall excellent ($R^2 > 0.99$). The value of E_a found for **10** is considerably lower than that for **3**, in agreement with the higher catalytic efficiency detected for the former during qualitative runs (Table 2, entries 3, 10, and 11). Eyring analysis was performed with the same data set (Table 3). As expected for a concerted six-centered mechanism, the large, negative activation entropy for **10** ($\Delta S^{\neq} = -206.0(6.6)$ J mol^{-1} K^{-1}) could tentatively be seen as diagnostic of a highly ordered transition state, as often cited for with oxophilic metals.[8,11,12] At the same time, the activation energy and entropy for **3** are quite different from those found for **10**, while these two different precatalysts are anticipated to generate the same active species. The moderate KIE ($k_{H_2}/k_{D_2} = 2.6$) observed for **3** perhaps reflects the fact that in the case of this amido precatalyst, the overall rate-limiting step consists in the preliminary acid-base reversible equilibrium (involving **3** and **S**) rather than any subsequent step in the actual catalytic cycle.

Table 3. Arrhenius and Eyring analyses in the temperature range 25–60 °C for the cyclohydroamination of **S** catalyzed by **3** and **10** in C_6D_6 ([**3**]/[**S**] = 1:20; [**10**]/[**S**] = 1:100).

	E_a [kJ mol^{-1}]	$\Delta H^{\neq}$ [kJ mol^{-1}]	$\Delta S^{\neq}$ [J mol^{-1} K^{-1}]
3	98.2(4.5)	95.4(4.5)	−13.2(13.8)
10	29.2(2.1)	26.7(2.1)	−206.0(6.6)

Based on literature precedents, and neglecting the potential role of THF, a mechanism for cyclohydroaminations catalyzed by Ba precatalysts **3** and **10** compatible with the rate law [Eq. (2)] and the determined activation parameters is proposed in Scheme 2.[19f] This mechanism is different from that we have recently presented for several aminophenolate Ae precatalysts, for which no dependence in substrate concentration was found, as expected for a rate-determining step consisting of the insertion of the polarized alkene into the Ae–N bond.[21]

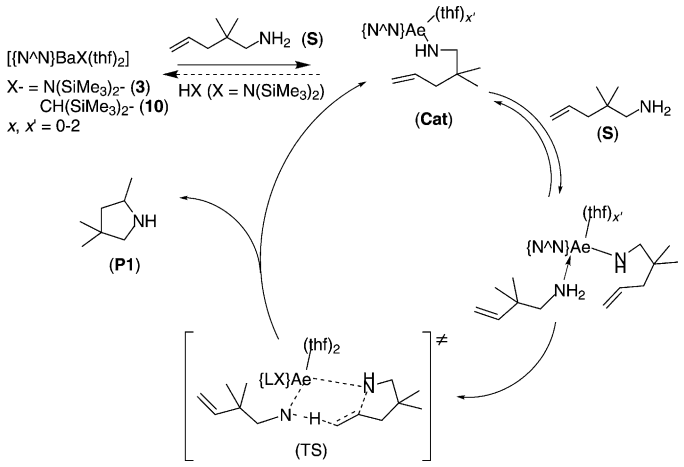

Scheme 2. Proposed mechanism for the cyclohydroamination of 1-amino-2,2-dimethyl-4-pentene (**S**) catalyzed by Ba-based precatalysts **3** and **10**.

Intermolecular and domino hydroamination reactions: The unique behavior of amido Ca, Sr, and Ba precatalysts supported by β-diketiminate (such as [{BDI}Ca{N(SiMe$_3$)$_2$}(thf)] (**6**) and its derivatives [{BDI}Ae{N(SiMe$_2$H)$_2$}(thf)$_x$] **13**–**15**), aminoether-phenolate and iminoanilide (such as **1**–**3**) ligand scaffolds during intermolecular hydroamination of activated alkenes (dienes, styrenics) has been reported in a preliminary communication,[20] and shall not be discussed in many details here. Complementary experiments have been performed with the new alkyl heteroleptic compounds **8**–**10**. Precatalyst loading of 2 mol % and neat substrates were used at 60 °C.

General lines can be drawn from the data displayed in Table 4. In agreement with the proposed theoretical models and experimental observations,[12] the reaction systematically proceeded with strict anti-Markovnikov regioselectivity. Precatalysts **1**–**3** promoted the hydroamination of styrene with benzylamine ([precatalyst]$_0$/[styrene]$_0$/[amine]$_0$ = 1:50:50) with high efficacy (entries 1–3), but contrary to anticipations based on DFT computations for homoleptic precatalysts for intermolecular reactions,[12] the catalytic activity improved regularly from Ca to Ba, that is, with increasing ionic radius. This trend is the opposite of that reported above for cyclohydroamination reactions, but it was confirmed with two other families of ancillary ligands.[20] In the series of amido precatalysts, the Ba complex **3** achieved near-complete conversion over 18 h (entry 3), the Ca (**1**) and Sr (**2**) complexes converted respectively 34 % and 71 % of the substrates (en-

Table 4. Representative data for the hydroamination of styrene with amines catalyzed by **1**–**5** and **8**–**10**.[a]

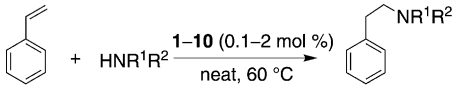

HNR^{1}R^2 = benzylamine or pyrrolidine

Entry	Precatalyst	Amine	time [min]	Conversion [%][b]
1	**1**	$BnNH_2$	1080	34
2	**2**	$BnNH_2$	1080	71
3	**3**	$BnNH_2$	1080	86
4	**1**	pyrrolidine	30	65
5	**2**	pyrrolidine	30	75
6	**3**	pyrrolidine	30	95
7[c]	**3**	pyrrolidine	120	85
8	**4**	pyrrolidine	30	0
9	**5**	pyrrolidine	30	82
10	**8**	pyrrolidine	5	28
11	**8**	pyrrolidine	30	90
12	**9**	pyrrolidine	5	85
13	**10**	pyrrolidine	5	97

[a] [precatalyst]$_0$/[styrene]$_0$/[amine]$_0$ = 1:50:50 unless otherwise specified, precatalyst: 10.0 μmol, 60 °C. [b] Conversion determined by ^{1}H NMR spectroscopy. [c] [**3**]$_0$/[styrene]$_0$/[amine]$_0$ = 1:500:500.

tries 1 and 2). Faster reaction rates were achieved with pyrrolidine, as 50 equivalents of substrates were transformed almost quantitatively by **3** within 30 min (entry 6); with $[\text{styrene}]_0/[\text{pyrrolidine}]_0/[\mathbf{3}]_0 = 500:500:1$, 85% of the substrates was converted in 2 h, with a corresponding turnover frequency of 212 h^{-1} (entry 7). As found for cyclohydroamination reactions, the new alkyl precatalysts **8**–**10** outclassed by far their amido analogues (Table 4, entries 4, 10, and 11; 5 and 12; 6 and 13), and the activity still decreased regularly according to Ba > Sr > Ca (compare entries 1–3, 4–6, or 10–13). Notably, the Ba complex **10** affords the most active (and yet fully regioselective) catalyst for intermolecular hydroamination of activated alkenes reported to date.[45] The Eu^{II} complex **5** exhibited catalytic activity matching that of its Sr analogue **2**, with 82% and 75% of the substrates respectively converted in 30 min for $[\text{styrene}]_0/[\text{pyrrolidine}]_0/[\text{precatalyst}]_0 = 50:50:1$ (entries 5 and 9). On the other hand, the Yb^{II} complex **4** was decomposed during intermolecular hydroamination reactions and eventually proved inefficient. The complex immediately oxidized in the presence of styrene and pyrrolidine (as evidenced by the rapid color change from purple to yellow concomitant with the formation of a precipitate, and the fact that exploitable NMR data could not be recorded), and the newly formed species (which could not be characterized) was entirely incapable of catalyzing the reaction. We double-checked that **4** was inert toward styrene (in particular polymerization of styrene was not seen under the chosen conditions) and pyrrolidine taken separately, and therefore it is only the combination of the two that leads to oxidation of **4**; similar observations were made when isoprene and/or benzylamine were employed. Note also that **4** did not decompose in the presence of mixtures of phosphine and activated alkenes (vide infra), and that **5** did not oxidize under the presence of amine and/or styrene. The different behaviors of **4** and **5** are certainly to be linked to the standard redox potential of their metal centers, with Yb^{II} complexes such as **4** being much more sensitive to oxidation ($E^0 = -1.05$ and -0.35 V for Yb^{3+}/Yb^{2+} and Eu^{3+}/Eu^{2+}, respectively). It is unclear why **4** should be sensitive toward mixtures of amines and activated alkenes, but not toward mixtures of phosphines and activated alkenes, or toward aminoalkenes (see above), even if the faculty of activated alkenes to attract electrons can certainly be evoked. We were unable to find literature precedent for such behavior, even if Roesky et al. have recently reported the oxidation (through disproportionation) of a bis(imidazolin-2-iminato)Yb^{II} complex that led to the formation of a crystallographically characterized bis(imidazolin-2-iminato)Yb^{III}-iodide complex.[46]

On the whole, under reactions conditions fairly similar for cyclohydroamination and intermolecular reactions, the former took place much more rapidly than the latter upon catalysis with **1**–**5** and **8**–**10**. Moreover, the order of activity switched with the nature (size) of the Ae metal between the two catalyzed reactions. The barium precatalyst **3**, for which the catalytic activity in the cyclohydroamination of aminoalkenes and the intermolecular hydroamination of activated alkenes with amines can be combined advantageously, was selected to catalyze the one-pot "domino" sequence consisting of the cyclohydroamination of **S** and subsequent hydroamination of styrene with the resulting 2,4,4-trimethylpyrrolidine (**P1**) (Scheme 3). Upon simultaneous mixing of **3**, **S**

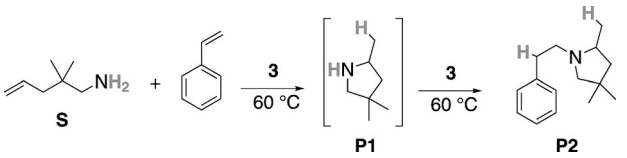

Scheme 3. One-pot "domino" cyclohydroamination-hydroamination sequence.

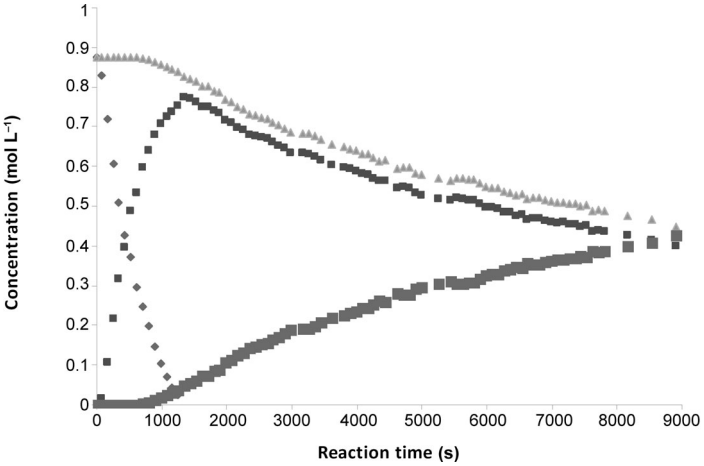

Figure 10. Plot of concentrations in styrene (▲), 1-amino-2,2-dimethyl-4-pentene (**S**; ◆), 2,4,4-trimethylpyrrolidine (**P1**, ■) and 2-(2,4,4-trimethylcyclopentyl)ethyl)benzene (**P2**; ■) versus reaction time during the one-pot "domino" synthesis of **P2** catalyzed by [{N^N}Ba{$N(SiMe_3)_2$}$(thf)_2$] (**3**). Reaction conditions: $[\text{styrene}]_0/[\mathbf{S}]_0/[\mathbf{3}]_0 = 50:50:1$, $[\mathbf{3}]_0 = 0.018$ M, 60 °C, solvent: C_6D_6, total volume (styrene + **S** + C_6D_6) = 0.6 mL.

and styrene in C_6D_6 ($[\text{styrene}]_0/[\mathbf{S}]_0/[\mathbf{3}]_0 = 50:50:1$, 60 °C), rapid consumption of the aminoalkene and concomitant formation of **P1** was monitored by ^{1}H NMR spectroscopy (Figure 10). The linear semi-logarithmic plot of $\ln([\mathbf{S}]_0/[\mathbf{S}]_t)$ versus reaction time suggested partial first-order in substrate concentration. The intermediate's concentration ($[\mathbf{P1}]_t$) rose to a maximum, then decayed until complete disappearance; consumption of $[\mathbf{P1}]_t$ and styrene occurred simultaneously with formation of 2-(2,4,4-trimethylcyclopentyl)ethyl)benzene (**P2**) through intermolecular hydroamination of styrene with **P1** catalyzed by **3**. Again, the semi-logarithmic plots of substrate consumption versus reaction time for **P1** and styrene were linear. Overall, the profile for the concentrations in **S**, **P1**, and **P2** (Figure 10) is characteristic of consecutive elementary reactions. This method represents an efficient tool for the synthesis of a wide range of non-symmetrical tertiary amines starting from readily available aminoalkenes and activated alkenes.[47]

Hydrophosphination reactions: Since hard, oxophilic nature of Ae and RE^{II} elements offers ideal conditions for the catalysis of C–P bond formation using soft HPR_2 phosphines, ability of **1**–**5** and **8**–**10** to catalyze the hydrophosphination of activated alkenes with secondary phosphines was interrogated.

In a preliminary set of experiments, the addition of $HPCy_2$ or $HPPh_2$ across the vinylic bond in styrene derivatives was examined with a catalyst loading of 2.0 mol% (Table 5). In all cases, the reactions afforded exclusively the anti-Markovnikov product. Reactions involving styrene and $HPCy_2$ were relatively slow, with substrate conversion in the range 31–50% after 18 h (entries 1–4). By comparison, reaction rates were much greater with the less basic $HPPh_2$ (Table 5, entries 5–20), with full conversion of the substrate being essentially achieved in as little as 3–15 min with the Ba derivatives **3** and **10** (entries 7 and 13). As found for intermolecular hydroamination, the order of catalytic activity decreased with the size of the metal according to $Ba > Sr \sim Eu^{II} > Ca \sim Yb^{II}$. No notable difference was found between Ae and RE^{II} metals with identical sizes (compare entries 5 and 8 as well as 6 and 9). Unlike seen for intermolecular hydroamination, no oxidation of the Yb^{II} precatalyst **4** was detected here, either with $HPCy_2$ (entry 4) or $HPPh_2$ (entry 8).

Table 5. Hydroamination of styrene with amines catalyzed by **1**–**5** and **8**–**10**.[a]

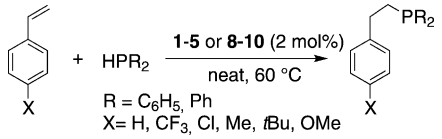

anti-Markovnikov

Entry	Precatalyst	HPR_2	X	time [min]	Conversion [%][b]
1	**1**	$HPCy_2$	H	1080	31
2	**2**	$HPCy_2$	H	1080	41
3	**3**	$HPCy_2$	H	1080	50
4	**4**	$HPCy_2$	H	1080	35
5	**1**	$HPPh_2$	H	15	42
6	**2**	$HPPh_2$	H	15	92
7	**3**	$HPPh_2$	H	15	>96
8	**4**	$HPPh_2$	H	15	45
9	**5**	$HPPh_2$	H	15	93
10	**8**	$HPPh_2$	H	3	20
11	**8**	$HPPh_2$	H	15	76
12	**9**	$HPPh_2$	H	3	55
13	**10**	$HPPh_2$	H	3	95
14	**1**	$HPPh_2$	CF_3	10	92
15	**1**	$HPPh_2$	Cl	10	80
16	**3**	$HPPh_2$	CF_3	5	80
17	**3**	$HPPh_2$	Cl	<10	95
18	**3**	$HPPh_2$	Me	15	79
19	**3**	$HPPh_2$	*t*Bu	30	44
20	**3**	$HPPh_2$	OMe	30	27

[a] $[precatalyst]_0/[styrene]_0/[phosphine]_0 = 1:50:50$, no solvent, precatalyst: 10.0 μmol, 60 °C. [b] Conversion determined by ^1H NMR spectroscopy.

The Ae-alkyl precatalysts **8**–**10** were more active than their Ae-amide congeners **1**–**3** (Table 5, entries 5 and 11, or also 7 and 13). Overall, these intermolecular hydrophosphination precatalysts, and in particular the barium ones **3** and **10**, are second to none in terms of activity and regioselectivity.[2d,7,13,17]

The Ba precatalysts afforded the highest apparent activity figures by some margin. The amido precatalyst **3**, albeit slightly less efficient than its alkyl analogue **10**, was the most suited to assess qualitatively the influence of substitution at the *para* position of the aromatic ring in the styrenic substrates, as reactions with the latter were too fast to be conveniently and reliably monitored (Table 5, entry 13).[48] The electron-withdrawing inductive effect of chlorine led to increased activity, as full conversion of *p*-Cl-styrene was achieved within less than 10 min (Table 5, entries 7 and 17). With the even more electron-withdrawing CF_3, high to complete conversions were now achieved with **10** or **8** within 5–10 min (Table 5, entries 14 and 16). By contrast, with electron-donating *para* substituents (Me, *t*Bu, or OMe, entries 18–20) lower reaction rates were measured, decreasing with increasing electron-donating strength according to $(CF_3 > Cl >)H > Me > tBu > OMe$. This recalls observations made independently by our group and that of Hill during the intermolecular hydroamination of styrene derivatives.[12b,20] These Ae-catalyzed intermolecular hydrophosphination reactions afford regiospecifically the anti-Markovnikov product, presumably through a rate-determining step consisting of insertion of the highly polarized double bond into the Ba–P bond as suggested by the empirically determined rate law (see below). The observed trend is compatible with this scenario for C–P bond formation since during the rate-determining step, deleterious electron-donating substituents at the *para* position of the styrene derivative tend to destabilize the developing negative charge on the benzylic (α) carbon atom, whereas electron-withdrawing *para*-substituents stabilize this growing negative charge and hence afford higher reaction rates (Figure 11). Yet one should note that EW *p*-groups most likely have a detrimental effect on the ability of the styrenic substrates to bind to the metal, so that the results of these experiments probably describe the global effect of several composite contributions.[48]

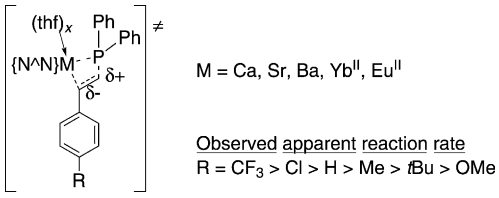

Figure 11. Proposed transition state and observed reactivity trend in the intermolecular hydrophosphination of *p*-substituted styrenics with $HPPh_2$ catalyzed by **1**–**5** or **8**–**10**.

Kinetic measurements were conducted to gain insight in the hydrophosphination of styrene with $HPPh_2$ catalyzed by

1–5 or **8–10**. In the presence of a high excess of styrene (as customarily done to maintain its concentration virtually unchanged), the plots of phosphine conversion versus reaction time were linear in all cases, indicating absence of dependence upon $[HPPh_2]$.[28,49] This was corroborated by examination of the turnover frequencies (TOF) for the hydrophosphination catalyzed by **1** at three different $HPPh_2$ concentrations spreading in a 4-fold range (88.3, 166.7, and 333.3 mM), all other parameters remaining unchanged: identical TOFs were found in all cases (24.0, 24.2, and 24.3 $mol_{product} \cdot mol_{Ca}^{-1} h^{-1}$ respectively). The apparent rate constants ($k_{app}^{\mathbf{1}}$) were also determined for different catalyst (in the range 1.90–58.5 mM) and styrene (between 1.34–5.25 M) concentrations. The corresponding semi-logarithmic plots of $\ln(k_{app}^{\mathbf{1}})$ versus $\ln([\mathbf{1}]_0)$ and $\ln(k_{app}^{\mathbf{1}})$ versus $\ln([styrene]_0)$ were both linear with slopes of 0.95 ($R^2 = 0.9768$) and 1.08 ($R^2 = 0.9908$),[28] indicating that the reaction kinetics followed first order in both precatalyst and styrene concentrations (Figures 12 and 13). The empirical rate law for the hydrophosphination of styrene with $HPPh_2$ catalyzed by **1** can therefore be expressed as in Equation (3).

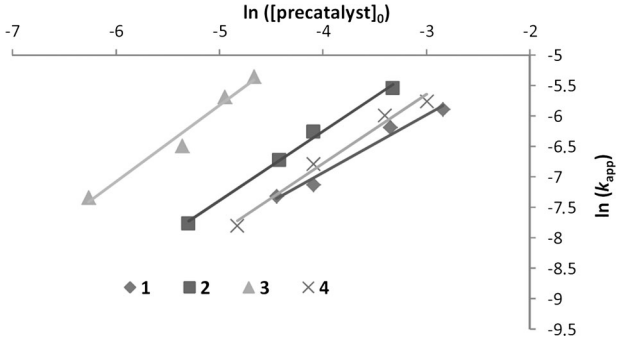

Figure 12. Plots of ln (k_{app}) versus ln([precatalyst]$_0$) for the intermolecular hydrophosphination of styrene and $HPPh_2$ catalyzed by [{N^N}M{N(SiMe$_3$)$_2$}(thf)$_x$] (M = Ca, $x = 1$, **1**; Sr, $x = 2$ **2**; Ba, $x = 2$ **3**; Yb^{II}, $x = 1$ **4**) at different precatalyst concentrations in the range 1.9 to 58.5 mM. Reaction conditions: **1**: 60 °C, $[styrene]_0 = 1.34$ M, $[styrene]_0$:$[HPPh_2]_0 = 10:1$, C_6D_6+Ph_2PH+styrene = 0.6 mL; **2**: 40 °C, $[styrene]_0 = 1.34$ M, $[styrene]_0$:$[HPPh_2]_0 = 10:1$, C_6D_6+Ph_2PH+styrene = 0.6 mL; **3**: 40 °C, $[styrene]_0 = 1.34$ M, $[styrene]_0$:$[HPPh_2]_0 = 10:1$, C_6D_6+Ph_2PH+styrene = 1.2 mL; **4**: 60 °C, $[styrene]_0 = 1.34$ M, $[styrene]_0$:$[HPPh_2]_0 = 10:1$, C_6D_6+Ph_2PH+styrene = 0.6 mL.

$$R_{HP} = k[HPPh_2]^0[styrene]^1[\mathbf{1}]^1 \quad (3)$$

Investigations performed for the Sr, Ba, and Yb^{II} precatalysts **2–4** provided the same outcome, and therefore the rate law given in Equation (3) can be extended to each of these.[50] The activation energy values, $E_a = 70.5(5.4)$ (**1**), 43.3(6.0) (**2**), 34.2(2.4), (**3**) and 60.7(5.4) (**4**) kJ mol^{-1}, were determined for **1–4** by an Arrhenius analysis performed in the temperature range 30–70 °C (Figure 14). These values were in good agreement with the qualitative trend disclosed in Table 5, that is, Ba > Sr > Ca ~ Yb, established already for hydrophosphination reactions.[51] The values of $\Delta S^{\neq}$ and $\Delta H^{\neq}$ were also calculated from the relevant Eyring plots (Table 6).

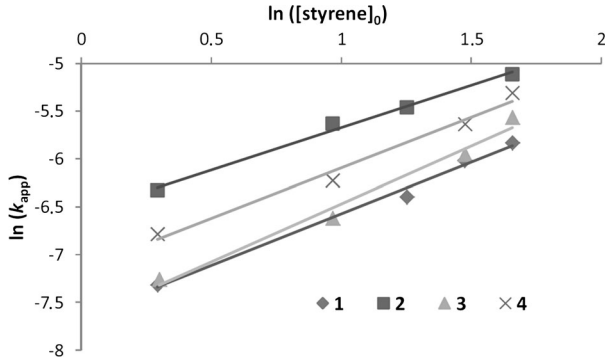

Figure 13. Plots of ln (k_{app}) versus ln([styrene]$_0$) for the intermolecular hydrophosphination of styrene and $HPPh_2$ catalyzed by [{N^N}M{N(SiMe$_3$)$_2$}(thf)$_x$] (M = Ca, $x = 1$ **1**; Sr, $x = 2$ **2**; Ba, $x = 2$ **3**; Yb^{II}, $x = 1$ **4**) at different styrene concentrations in the range 1.34 to 5.25 M. Reaction conditions: **1**: 10.0 μmol, 60 °C, $[\mathbf{1}]_0/[HPPh_2]_0 = 1:8$, C_6D_6+$HPPh_2$+styrene = 0.6 mL; **2**: 10 μmol; 40 °C, $[\mathbf{2}]_0/[HPPh_2]_0 = 1:8$, C_6D_6+$HPPh_2$+styrene = 0.6 mL; **3**: 5.0 μmol; 40 °C, $[\mathbf{3}]_0/[HPPh_2]_0 = 1:32$, C_6D_6+$HPPh_2$+styrene = 1.2 mL; **4**: 10.0 μmol, 60 °C, $[\mathbf{4}]_0/[HPPh_2]_0 = 1:8$, C_6D_6+$HPPh_2$+styrene = 0.6 mL.

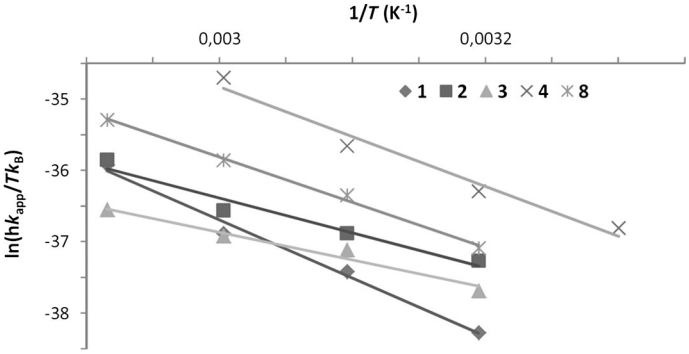

Figure 14. Eyring plots of ln ((k_{app}h)/(k_BT)) versus 1/T for the intermolecular hydrophosphination of styrene and $HPPh_2$ catalyzed by [{N^N}M{N(SiMe$_3$)$_2$}(thf)$_x$] (M = Ca, $x = 1$, **1**; Sr, $x = 2$ **2**; Ba, $x = 2$ **3**; Yb^{II}, $x = 1$ **4**) or [{N^N}Ca{CH(SiMe$_3$)$_2$}(thf)] (**8**) in the temperature range 303–343 K. Reaction conditions: **1**: 10.0 μmol, $[\mathbf{1}]_0/[styrene]_0/[HPPh_2]_0 = 1:80:8$, C_6D_6+$HPPh_2$+styrene = 0.6 mL; **2**: 3.0 μmol; $[\mathbf{2}]_0/[styrene]_0/[HPPh_2]_0 = 1:270:27$, C_6D_6+$HPPh_2$+styrene = 0.6 mL; **3**: 2.3 μmol, $[\mathbf{3}]_0/[styrene]_0/[HPPh_2]_0 = 1:700:70$, C_6D_6+$HPPh_2$+styrene = 1.2 mL; **4**: 10.0 μmol, $[\mathbf{4}]_0/[styrene]_0/[HPPh_2]_0 = 1:80:8$, C_6D_6+$HPPh_2$+styrene = 0.6 mL; **8**: $[\mathbf{8}]_0/[styrene]_0/[HPPh_2]_0 = 1:80:8$, C_6D_6+$HPPh_2$+styrene = 0.6 mL.

Based on our experimental findings, the mechanism represented in Scheme 4 (which ignores the potential influence of THF in these precatalysts as its exact role could not be assessed, even if as before the ^{1}H NMR spectra of in situ monitored hydrophosphination reactions seemed to hint that THF was released under catalytic conditions) is proposed for the hydrophosphination of styrene derivatives with secondary phosphines catalyzed by Ae and RE^{II} precatalysts **1–5** and **8–10**. In such mechanism, two essential parameters will affect the overall kinetics: the amount of catalytically active species existing in the medium, and the

Table 6. Activation energy (E_a), enthalpy ($\Delta H^{\neq}$) and entropy ($\Delta S^{\neq}$) of the hydrophosphination of styrene with diphenylphosphine catalyzed by complexes **1**–**4** and **8**.

Entry	Precatalyst	E_a [kJ mol^{-1}]	$\Delta H^{\neq}$ [kJ mol^{-1}]	$\Delta S^{\neq}$ [J mol^{-1} K^{-1}]
1[a]	**1**	70.5(5.4)	67.7(5.4)	−101.8(16.5)
2[b]	**2**	43.3(6.0)	40.6(6.0)	−180.7(18.4)
3[c]	**3**	34.2(2.4)	31.5(2.4)	−212.1(7.3)
4[a]	**4**	60.7(5.4)	58.0(5.4)	−115.4(22.3)
5[a]	**8**	55.4(2.5)	52.7(2.5)	−139.6(7.7)

[a] Precatalyst: 10.0 μmol; [precatalyst]$_0$/[styrene]$_0$/[HPPh$_2$]$_0$ = 1:80:8, C_6D_6 + Ph_2PH + styrene = 0.6 mL; [b] **2**: 3.0 μmol; [**2**]$_0$/[styrene]$_0$/[HPPh$_2$]$_0$ = 1:270:27, C_6D_6 + Ph_2PH + styrene = 0.6 mL; [c] **3**: 2.3 μmol; [**3**]$_0$/[Styrene]$_0$/[HPPh$_2$]$_0$ = 1:700:70, C_6D_6 + Ph_2PH + styrene = 1.2 mL.

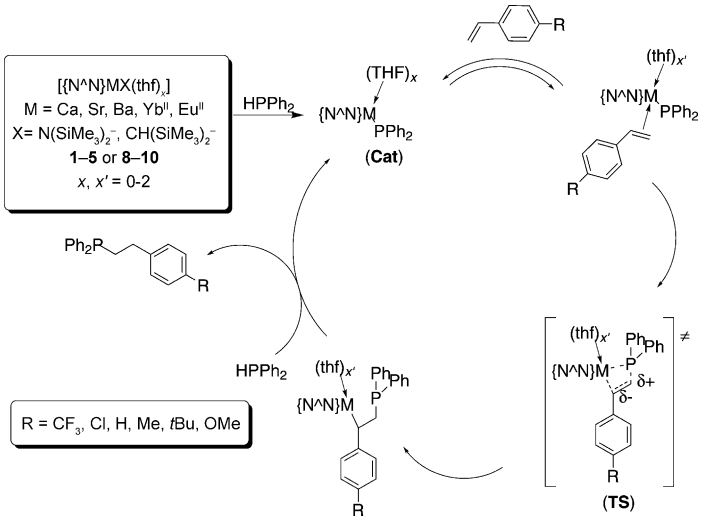

Scheme 4. Proposed catalytic cycle for the hydrophosphination of styrene derivatives with diphenylphosphine catalyzed by Ae and RE^{II} precatalysts (**1**–**5** and **8**–**10**).

nature of the rate-determining step, which on account of the zero-dependence in [phosphine] we propose consists of insertion of the polarized alkene into the metal–phosphide bond. The higher acidity of $HPPh_2$ (pK_a (DMSO) = 22.9; pK_a (THF) = 21.7) compared with that of $HPCy_2$ (pK_a (DMSO) = 34.6; pK_a (THF) = 35.7)[52] is consistent with the much greater reaction rates observed with the former, as the catalytic active species (**Cat**) is first generated by protonolysis of the M−X bond with the secondary phosphine. The extent of deprotonation/reprotonation equilibria also explains the somewhat better efficiency discerned for Ae-alkyl precatalysts **8**–**10** (X = $CH(SiMe_3)_2^-$) in comparison with the Ae-amides **1**–**3** and their RE^{II} analogues **4** and **5** (X = $N(SiMe_3)_2^-$): this initial acid–base equilibrium shifts very much toward the formation of **Cat** with the strongly basic hydrocarbyl group $CH(SiMe_3)_2^-$, whereas the amount of catalytically active species that exists at a given time of the catalyzed reaction will be lesser for the comparatively more acidic $N(SiMe_3)_2^-$ (pK_a ($HN(SiMe_3)_2$/$N(SiMe_3)_2^-$ = 25.8 in DMSO).[53,54] As discussed above, the mechanism displayed in Scheme 4 is in agreement with the overall order of apparent activity detected for the *para*-substituent on the styrenic substrate (R = Cl > H > Me > *t*Bu > OMe), and with the strict 2,1-anti-Markovnikov regiospecifity observed in these catalyzed reactions. To our knowledge, there are only two pertinent examples of Ae-catalyzed hydrophosphination of alkenes, but the mechanisms at work have not been detailed.[13,17] The catalytic cycle herein suggested relates to that of Marks et al. for the cyclohydrophosphination of phosphinoalkenes.[7,55] We have tried but so far not been able to isolate the putative species (**Cat**). Yet, Hill et al. have isolated and characterized the related [{BDI}-Ca(PPh$_2$)(thf)] after equimolar reaction of **6** and $HPPh_2$.[13] Although kinetically unstable at elevated temperature, this complex was able to catalyze (albeit slowly) styrene/$HPPh_2$ hydrophosphination, and this finding combined with our study provide strong claim for the plausibility of the proposed mechanism. Moreover, like **6**, the tetramethyldisilazide derivatives [{BDI}Ae{N(SiMe$_2$H)$_2$}(thf)$_2$] **13**–**15** are efficient hydrophosphination precatalysts, being outclassed only by **1**–**3** and **8**–**10** and showing the same regioselectivity as them.[20]

The catalysis of isoprene hydrophosphination was examined next. The addition of $HPPh_2$ was very rapid at 60 °C with a catalyst loading of 2.0 mol % in neat substrates, but was not fully regioselective (Table 7). The Sr and Ba precatalysts proved much more active than the Ca-based ones, but under the chosen conditions it was not possible to discriminate between Sr and Ba, as full conversion was always achieved within 9 min for **2**–**3** as well as **9**–**10**, nor between amido and hydrocarbyl reactive groups. The regioselectivity varied largely with the identity of the metal. Whereas the Ca precatalysts **1** and **8** afforded preponderantly the 3,4-addition product, the Ba complexes **3** and **10** gave a 3:1 regioselectivity in favor of the 1,4-addition product. In the case of the Sr precatalysts **2** and **9**, the product of 1,4-addition was very modestly favored. Such moderate levels of regioselectivity contrast starkly with the entire 2,1-regiospecificity seen for the intermolecular hydroamination of isoprene with pyrrolidine catalyzed by **1**–**3**;[20] yet Hill et al. reported near-

Table 7. Isoprene/$HPPh_2$ hydrophosphination catalyzed by **1**–**3** and **8**–**10**.[a]

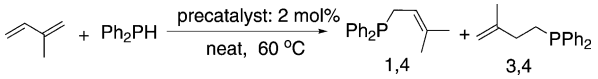

Entry	Precatalyst	time [min]	Conversion [%][b]	Regioselectivity 1,4	3,4
1	**1**	15	94	26	74
2	**8**	15	96	25	75
3	**2**	9	97	40	60
4	**9**	9	98	39	61
5	**3**	9	99	74	26
6	**10**	9	99	73	27

[a] Reaction conditions: [precatalyst]$_0$/[isoprene]$_0$/[HPPh$_2$]$_0$ = 1:75:50, no solvent (bulk), precatalyst: 10.0 μmol, 60 °C. [b] Conversion determined by ^{1}H NMR spectroscopy.

Table 8. Hydrophosphination of activated alkenes catalyzed by [{N^N}Ca{N(SiMe$_3$)$_2$}(thf)] (**1**), [{N^N}Ba{N(SiMe$_3$)$_2$}(thf)$_2$] (**3**) and [{N^N}-Yb^{II}{N(SiMe$_3$)$_2$}(thf)] (**4**).[a]

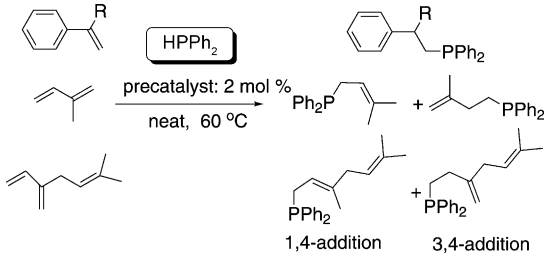

Entry	Substrate	Time [min]	**1** conv. [%][b]	**1** regio.[b] 1,4	**1** 3,4	**3** conv. [%][b]	**3** regio.[b] 1,4	**3** 3,4	**4** conv. [%][b]	**4** regio.[b] 1,4	**4** 3,4
1[c]	isoprene	15	94	26	74	99	74	26	98	28	72
2	myrcene	15	96	51	49	99	83	17	97	53	47
3	α-methylstyrene	240	2	–	–	90	–	–	6	–	–
4	styrene	15	42	–	–	>96	–	–	45	–	–

[a] Reactions conditions: [precatalyst]$_0$/[alkene]$_0$/[HPPh$_2$]$_0$=1:50:50, precatalyst: 10.0 μmol, 60 °C unless otherwise specified. [b] Conversion and selectivity determined by ^{1}H NMR spectroscopy. [c] [precatalyst]$_0$/[isoprene]$_0$/[HPPh$_2$]$_0$=1:75:50. [d] C_6D_6: 0.45 mL.

identical regioselectivity to that observed with **1**/**8** for the hydrophosphination of isoprene/HPPh$_2$ catalyzed by **6**.[13] For a given metal, the product distribution was not altered with the nature of the basic X group, consistent with no involvement of this moiety in the catalytically active species (Scheme 4).

The influence of the size of the metal on the regioselectivity of hydrophosphination of a variety of other activated substrates was probed (Table 8). Under the chosen conditions (2.0 mol % precatalyst loading), the Yb^{II} and Ca complexes displayed poor (Table 8, entry 3, R=Me, α-methylstyrene) to moderate (Table 8, R=H, entry 4, styrene) activities in the hydrophosphination of styrene derivatives, whereas even under such mild conditions the Ba-based **3** exhibited high catalytic activity and complete anti-Markovnikov regiospecificity. Isoprene (entry 1) and myrcene (entry 2) afforded fast reactions, with complete conversion being observed in all cases within 15 min. The Yb^{II} (**4**) and Ca (**1**) displayed the same selectivity, with as previously in bulk reactions a 1:3 ratio in favor of the 3,4-addition product in the case of isoprene, and total absence of regioselectivity with myrcene. As found before, the Ba precatalyst **3** disclosed regioselectivity of its own, leading prominently to the formation of the 1,4-addition product both for myrcene and isoprene. Note that with all precatalysts, the non-activated (non-conjugated) C=C moiety in myrcene was fully inert toward hydrophosphination. In a screening experiment, **3** effectively catalyzed the hydrophosphination of diphenylethyne with HPPh$_2$ (82 % conversion was observed after 4 h at 60 °C, with [**3**]$_0$/[diphenylethyne]$_0$/[HPPh$_2$]$_0$=1:50:50 in 0.45 mL of C_6D_6), leading to the formation of 1,2-diphenylethene with a *E*/*Z* ratio of 65:35. Finally, attempts to carry out hydrophosphination of 2-vinylpyridine with **1**–**3** were unfruitful, and instead extremely fast and exothermic polymerization of the vinylic substrate was observed (formation of a gel was observed in a few seconds) under a range of conditions (T_0=25–60 °C).

Conclusion

The synthesis, solid-state structures, and catalytic performances of several alkyl and amide complexes of Ae and RE^{II} metals supported by a bulky iminoanilide ligand have been detailed. These heteroleptic complexes are fully stable in solution, and in particular they are not prone to Schlenk-type equilibria that often plague the coordination and reactivity chemistries of these large and highly oxophilic elements. The complexes [{N^N}Ae{CH(SiMe$_3$)$_2$}(thf)$_x$] constitute in particular the first complete set of heteroleptic alkyl complexes for the large alkaline earth metals Ca, Sr, and Ba.

These complexes display high aptitude in the catalysis of three key transformations: the cyclohydroamination of aminoalkenes, and the intermolecular hydroamination and hydrophosphination of activated alkenes (conjugated dienes, styrene derivatives). Except in one instance where a peculiar case of immediate oxidation of the Yb^{II} was observed upon mixing with styrene (or isoprene) and pyrrolidine (or benzylamine), the RE^{II} precatalysts did not undergo oxidation under catalytic conditions, and essentially showed the same ability as their direct alkaline earth cousins with almost identical ionic radii (Yb^{II} and Ca; Eu^{II} and Sr), both in terms of selectivity and catalytic activity. In this regard, the iminoanilide ligand {N^N}$^-$ proved particularly efficient for stabilizing redox active RE^{II} centers, as compared with other ancillaries. Overall, the complexes based on Ca (and Yb^{II}), Sr (and Eu^{II}), and Ba represent some of the most efficient precatalysts reported to date for the considered organic transformations. Full anti-Markovnikov regiospecificity was observed in the case of intermolecular hydroamination and hydrophosphination of styrene derivatives, whereas ring-closure is also strictly regioselective (5-*exo*-trig) during the cyclohydroamination of terminal aminoalkenes. The selectivity is lesser during the hydrophosphination of dienes, and it depends on the size of the metal. If the size of the metal did

Table 9. Overview of hydroelementation reactions catalyzed by heteroleptic iminoanilide Ae precatalysts [{N^N}AeX(thf)$_x$] **1**–**3** and **8**–**10** (Ae = Ca, Sr, Ba; X$^-$ = CH(SiMe$_3$)$_2^-$, N(SiMe$_3$)$_2^-$; x = 1–2).

	Cyclohydroamination[a]	Intermolecular hydroamination	Intermolecular hydrophosphination
reactive group	CH(SiMe$_3$)$_2^-$ > N(SiMe$_3$)$_2^-$	CH(SiMe$_3$)$_2^-$ > N(SiMe$_3$)$_2^-$	CH(SiMe$_3$)$_2^-$ > N(SiMe$_3$)$_2^-$
metal size	Ca > Sr > Ba	Ca < Sr < Ba	Ca < Sr < Ba
kinetic rate law	k[M]^1[aminoalkenes]^1	k[M]^1[styrene]^1[amine]^1	k[M]^1[styrene]^1[phosphine]^0
maximal TOF	50.0 mol$_{prod}$ mol$_{Ca}^{-1}$ min^{-1}[b]	9.7 mol$_{prod}$ mol$_{Ba}^{-1}$ min^{-1}[c]	15.8 mol$_{prod}$ mol$_{Ba}^{-1}$ min^{-1}[d]

[a] M = metal precatalyst. [b] Non-optimized, obtained with **8**, Table 2, entry 8. [c] Obtained with **10**, Table 4, entry 13. [d] Obtained with **10**, Table 5, entry 13.

not influence the stability of the complexes, it was found to play a crucial role on catalytic activity. The alkyl compounds proved better catalyst precursors than their amido analogues. Following these considerations, [{N^N}Ba{N(SiMe$_3$)$_2$}(thf)$_2$] (**3**) and especially [{N^N}Ba{CH(SiMe$_3$)$_2$}(thf)$_2$] (**10**) emerged as the most competent precatalysts for the intermolecular version of these catalyzed reactions.

Mechanistic details and reactivity trends, which sometimes appear conflicting, were revealed in the course of this study (Table 9). During cyclohydroamination reactions, the catalytic activity decreases when descending in the column of Ae metals (Ba < Sr < Ca); this is in agreement with other reports.[14,16,21] Rather unusually, the rate law that was determined indicated first order dependence upon catalyst and susbstrate concentrations [Eq. (2)]; a different rate-law, with zeroth order dependence upon [substrate], was for instance presented for some aminophenolate Ca–Ba precatalysts.[21] A mechanism is proposed for the cyclohydroamination catalyzed by the iminoanilide Ae complexes, in which the transition state does not correspond to insertion of the polarized alkene into the metal–N bond, as often observed for lanthanide precatalysts,[2a–b,3,8] but instead consists in a highly ordered 6-centered structure with ring-closure and N–C bond formation occurring concomitantly with the transfer of a proton from a second coordinated molecule of substrate (Scheme 2). This is reminiscent of Sadow's recent report for the Mg-catalyzed cyclohydroamination of aminoalkenes,[19f] and is also very similar to the mechanism proposed in our preliminary communication on the intermolecular hydroamination of activated alkenes.[20] For this latter catalyzed reaction, the empirically determined kinetic rate law was of the first order in each of the three components [precatalyst, styrene, and amine; Eq. (1)] and a very large kinetic isotope effect ($k_{app}^{H_2}/k_{app}^{D_2}$ = 6.8–7.3) was measured.[20] However, in this case the reactivity decreased systematically according to Ba > Sr > Ca. Although it was contrary to expectations mostly based on theoretical calculations for homoleptic Ae precatalysts,[12] this trend was not a fortuitous isolated case, as it was revealed for three complete families of heteroleptic Ae complexes bearing a β-diketiminate (**13**–**15**), aminophenolate or iminoanilide ligand (**1**–**3**). The investigations related to the intermolecular hydrophosphination of styrene derivatives unveiled still different insight. The same reactivity versus metal size relationship as that disclosed for intermolecular hydroamination was observed: Ba > Sr(~Eu^{II}) > Ca(~Yb^{II}). Nonetheless, the kinetic rate law was different, with orders of 0, 1, and 1 found respectively for phosphine, styrene, and precatalyst concentrations [Eq. (3)]. Reaction rates for hydrophosphination varied according to CF$_3$ > Cl > H > Me > tBu > OMe upon introduction of substituents at the *para* position of the aromatic ring of the styrene derivative. The combination of this trend and the complete anti-Markovnikov regioselectivity of the addition is seen as being consistent with a transition state such as that depicted in Figure 11 and Scheme 4, with a growing negative charge on the benzylic carbon atom that is stabilized with increasing efficiency upon introduction of *para*-substituents of higher electron-withdrawing strength; nonetheless, it is important to take the amount of catalytically active species (generated by protonolysis of the M–X bond with the acidic substrate) existing at any given time into account when the apparent reaction rates and precatalyst efficiency are compared. The observed kinetic rate law agrees with the mechanistic scenario proposed for RE^{III}-catalyzed cyclohydrophosphination of phosphinoalkenes,[7] involving a rate-determining step consisting of insertion of the polarized C=C double bond in the metal–P(phosphide) bond.

Examination of the specificities for these catalyzed alkene hydroelementation reactions (Table 9) highlights rich, yet diverse features that are not yet well understood. The conflicting metal size versus catalytic activity relationships observed for intra- and intermolecular reactions obviously spring to mind, and so do the discrepancies observed between precatalysts based on the same metal but carrying different ancillary ligands.[21] The input of theoretical calculations will now be valuable to assess the finesses of Ae-catalyzed hydroelementations, and we will direct our efforts in this aim. In view of the somewhat limited number of truly efficient (pre)catalysts for intermolecular hydrophosphination (or in fact C–P bond formation)[1,2b,d,5,7] and despite the considerable synthetic challenges associated to these metals, it seems fit to consider these new (and related)[13,17,56] alkaline earth complexes as a most valuable addition to the arsenal of tools available to synthetic organometallic and organic chemists. The rare ability of these complexes to catalyze a domino cyclohydroamination/intermolecular hydroamination sequence opens up new opportunities, and future efforts will also be aimed at extending this sequential approach to a variety of combinations of hydroelementation reactions.

Experimental Section

All manipulations were performed under inert atmosphere using standard Schlenk techniques or in a Jacomex glovebox (O_2 < 1 ppm, H_2O <

5 ppm) for catalyst loading. NMR spectra were recorded on Bruker AC-300, AC-400 and AM-500 spectrometers. All chemicals shifts were determined using residual signals of the deuterated solvents. Assignment of the signals was carried out using 1D (^{1}H, ^{13}C{^{1}H}) and 2D (COSY, HMBC, HMQC) NMR experiments. Elemental analyses were performed on a Carlo Erba 1108 Elemental Analyser instrument at the London Metropolitan University by Stephen Boyer and were the average of a minimum of two independent measurements. CaI_2, SrI_2, BaI_2 (anhydrous beads, 99.995%) were purchased from Aldrich and used as received. Ytterbium and europium was purchased from Strem. $HN(SiMe_3)_2$ (Acros) was dried over activated 3 Å molecular sieves and distilled under reduced pressure prior to use. $[YbI_2(thf)_2]$ and $[EuI_2(thf)_2]$ were synthesized according to the literature.[57] Styrene, 4-chlorostyrene, 4-methoxystyrene, 4-methylstyrene, 4-*tert*-butylstyrene, 4-trifluoromethylstyrene, 2-vinylpyridine, isoprene, pyrrolidine, α-methylstyrene, and myrcene were purchased from Aldrich, Acros or ABCR. All were vacuum-distilled over CaH_2 and then were degassed by freeze-pump-thaw methods. Diphenylphosphine and dicyclohexylphosphine were purchased from Aldrich and used as received. THF was distilled under argon from Na/benzophenone prior to use. Other solvents (pentane, toluene, dichloromethane, Et_2O) were collected from MBraun SPS-800 purification alumina columns. Deuterated solvents (Eurisotop, Saclay, France) were stored in sealed ampoules over 3 Å molecular sieves and degassed by several freeze-thaw cycles. [{N^N}Ae{N(SiMe$_3$)$_2$}(thf)] (**1**–**3**), [{BDI}Ca{N(SiMe$_3$)$_2$}(thf)] (**6**), [{BDI}Yb^{II}{N(SiMe$_3$)$_2$}(thf)] (**7**), and $KCH(SiMe_3)_2$, were synthesized according to published procedures.[15,20,26,58]

[{N^N}Yb{N(SiMe$_3$)$_2$}(thf)] (4): A mixture of {N^N}H (0.21 g, 0.48 mmol) and $KN(SiMe_3)_2$ (0.19 g, 0.96 mmol) in THF (20 mL) was stirred at room temperature. After 1 h, it was added to a suspension of $[YbI_2(thf)_2]$ (0.25 g, 0.50 mmol) in THF (10 mL). The reaction mixture was vigorously stirred for 2.5 h. The solvent was then removed in vacuo and the residue was extracted with pentane (50 mL). Filtration followed by evaporation of the volatile components afforded a powder which was dried under reduce pressure to give **4** as a dark purple powder (0.29 g, 68%). Dark purple crystals of **4** suitable for single-crystal X-ray crystallography were obtained overnight by storage of a concentrated pentane solution at −30 °C. ^{1}H NMR (C_6D_6, 298 K, 500.13 MHz): δ = 8.17 (s, 1H; C*H*=N), 7.27 (d, $^3J_{HH}$ = 7.0 Hz, 2H; NC$_6$*H*$_3$), 7.21 (t, $^3J_{HH}$ = 6.9 Hz, 1HM NC$_6$*H*$_3$), 7.16 (overlapping signals, 3H; NC$_6$*H*$_3$), 7.06 (dd, $^3J_{HH}$ = 7.9 Hz, $^4J_{HH}$ = 1.6 Hz, 1H; C$_6$*H*$_4$), 6.90 (td, $^3J_{HH}$ = 7.8 Hz, $^4J_{HH}$ = 1.7 Hz, 1H; C$_6$*H*$_4$), 6.31 (d, $^3J_{HH}$ = 8.8 Hz, 1H; C$_6$*H*$_4$), 6.25 (t, $^3J_{HH}$ = 6.8 Hz, 1H; C$_6$*H*$_4$), 3.33 (overlapping m, 4H; OC*H*$_2$CH$_2$, and 4H; C*H*(CH$_3$)$_2$), 1.36 (d, $^3J_{HH}$ = 6.2 Hz, 6H; CH(C*H*$_3$)$_2$), 1.35 (d, $^3J_{HH}$ = 6.2 Hz, 6H; CH(C*H*$_3$)$_2$), 1.20 (d, $^3J_{HH}$ = 6.7 Hz, 6H; CH(C*H*$_3$)$_2$), 1.17 (d, $^3J_{HH}$ = 6.7 Hz, 6H; CH(C*H*$_3$)$_2$), 1.07 (br m, 4H; OCH$_2$C*H*$_2$), 0.07 ppm (s, 18H; Si(C*H*$_3$)$_3$). ^{13}C{^{1}H} NMR (C_6D_6, 298 K, 125.76 MHz): δ = 171.0 (*C*H=N), 160.1 (*i*-N=CH*C*$_6$H$_4$), 149.6 (*i*-N*C*$_6$H$_3$), 147.8 (*i*-N*C*$_6$H$_3$), 144.2 (*o*-N*C*$_6$H$_3$), 141.4 (*o*-N*C*$_6$H$_3$), 138.9 (*C*$_6$H$_4$), 133.8 (*C*$_6$H$_4$), 126.8 (*p*-N*C*$_6$H$_3$), 125.5 (*m*-N*C*$_6$H$_3$), 124.9 (*p*-N*C*$_6$H$_3$), 124.8 (*m*-N*C*$_6$H$_3$), 120.7 (*C*$_6$H$_4$), 118.4 (*i*-N*C*$_6$H$_4$), 112.8 (*C*$_6$H$_4$), 70.1 (O*C*H$_2$CH$_2$), 29.4 (*C*H(CH$_3$)$_2$), 29.0 (*C*H(CH$_3$)$_2$), 26.5 (CH(*C*H$_3$)$_2$), 26.3 (CH(*C*H$_3$)$_2$), 25.7 (CH(*C*H$_3$)$_2$), 25.5 (OCH$_2$*C*H$_2$), 23.9 (CH(*C*H$_3$)$_2$), 6.1 ppm (Si(*C*H$_3$)$_3$); elemental analysis calcd (%) for $C_{41}H_{65}N_3OSi_2Yb$ (845.18 g mol^{-1}): C 58.26, H 7.75, N 4.97; found: C 58.20, H 7.80, N 4.85.

[{N^N}Eu{N(SiMe$_3$)$_2$}(thf)$_2$] (5): Following a procedure similar to that described above for **4**, the reaction of {N^N}H (0.15 g, 0.34 mmol), $KN(SiMe_3)_2$ (0.14 g, 0.70 mmol), and $[EuI_2(thf)_2]$ (0.20 g, 0.36 mmol) afforded **5** (0.18 g, 60%) as a dark red powder. Single crystals of **5** were grown from a pentane solution at −30 °C. Elemental analysis calcd (%) for $C_{45}H_{73}N_3O_2Si_2Eu$ (896.22 g mol^{-1}): C 60.31, H 8.21, N 4.69: found: C 60.20, H 8.24, N 4.70.

[{N^N}Ca{CH(SiMe3)2}(thf)] (8): THF (20 mL) was added to a mixture of {N^N}H (0.76 g, 1.73 mmol) and $KCH(SiMe_3)_2$ (0.69 g, 3.48 mmol). The reaction mixture was stirred at room temperature for 1 h, and was then added to a suspension of CaI_2 (0.52 g, 1.77 mmol) in THF (20 mL). After stirring at room temperature for 2.5 h, the solvent was pumped off under vacuum and the residue was extracted with pentane (50 mL). After filtration, the volatiles were removed in vacuo to afford **8** (0.86 g, 70%) as a yellow solid. ^{1}H NMR (C_6D_6, 298 K, 500.13 MHz): δ = 8.02 (s, 1H; C*H*=N), 7.31 (d, $^3J_{HH}$ = 7.0 Hz, 2H; NC$_6$*H*$_3$), 7.27 (t, $^3J_{HH}$ = 6.9 Hz, 1H; NC$_6$*H*$_3$), 7.16 (overlapping signals, 3H; NC$_6$*H*$_3$), 7.00 (d, $^3J_{HH}$ = 7.7 Hz, 1H; C$_6$*H*$_4$), 6.82 (t, $^3J_{HH}$ = 7.8 Hz, 1H; C$_6$*H*$_4$), 6.27 (d, $^3J_{HH}$ = 8.9 Hz, 1H; C$_6$*H*$_4$), 6.24 (t, $^3J_{HH}$ = 7.3 Hz, 1H; C$_6$*H*$_4$), 3.46 (br m, 4H; OC*H*$_2$CH$_2$), 3.25 (m, 2H; C*H*(CH$_3$)$_2$), 3.10 (m, 2H; C*H*(CH$_3$)$_2$), 1.35 (d, $^3J_{HH}$ = 6.8 Hz, 6H; CH(C*H*$_3$)$_2$), 1.34 (d, $^3J_{HH}$ = 6.6 Hz, 6H; CH(C*H*$_3$)$_2$), 1.18 (d, $^3J_{HH}$ = 6.7 Hz, 6H; CH(C*H*$_3$)$_2$), 1.13 (d, $^3J_{HH}$ = 6.8 Hz, 6H; CH(C*H*$_3$)$_2$), 1.10 (br m, 4H; OCH$_2$C*H*$_2$), −0.01 (s, 18H; CH(Si(C*H*$_3$)$_3$)$_2$), −1.84 ppm (s, 1H; C*H*(Si(CH$_3$)$_3$)$_2$); ^{13}C{^{1}H} NMR (C_6D_6, 298 K, 125.76 MHz): δ = 172.3 (*C*H=N), 160.1 (*i*-N=CH*C*$_6$H$_4$), 149.6 (*i*-N*C*$_6$H$_3$), 146.5 (*i*-N*C*$_6$H$_3$), 144.3 (*o*-N*C*$_6$H$_3$), 141.1 (*o*-N*C*$_6$H$_3$), 139.3 (*C*$_6$H$_4$), 134.1 (*C*$_6$H$_4$), 127.0 (*p*-N*C*$_6$H$_3$), 125.6 (*m*-N*C*$_6$H$_3$), 125.5 (*p*-N*C*$_6$H$_3$), 124.8 (*m*-N*C*$_6$H$_3$), 119.5 (*C*$_6$H$_4$), 117.0 (N*C*$_6$H$_4$), 112.4 (*C*$_6$H$_4$), 70.0 (O*C*H$_2$CH$_2$), 29.6 (*C*H(CH$_3$)$_2$), 29.0 (*C*H(CH$_3$)$_2$), 26.3 (CH(*C*H$_3$)$_2$), 26.1 (CH(*C*H$_3$)$_2$), 25.7 (CH(*C*H$_3$)$_2$), 25.3 (OCH$_2$*C*H$_2$), 23.5 (CH(*C*H$_3$)$_2$), 14.8 (*C*H(Si(CH$_3$)$_3$)$_2$), 6.3 ppm (CH(Si(*C*H$_3$)$_3$)$_2$); elemental analysis (%) calcd for $C_{42}H_{66}N_2OSi_2Ca$ (711.24 g mol^{-1}): C 70.93, H 9.35, N 3.94; found: C 70.90, H 9.28, N 3.84.

[{N^N}Sr{CH(SiMe$_3$)$_2$}(thf)$_2$] (9): Following a procedure similar to that described for **8**, the reaction of {N^N}H (0.63 g, 1.43 mmol) and $KCH(SiMe_3)_2$ (0.57 g, 2.87 mmol) with SrI_2 (0.50 g, 1.46 mmol) afforded **9** (0.73 g, 62%) as a yellow powder. Yellow crystals of **9**·C_5H_{12} suitable for single-crystal X-ray crystallography were obtained overnight by storage of a concentrated pentane solution at −30 °C. ^{1}H NMR (C_6D_6, 298 K, 500.13 MHz): δ = 8.02 (s, 1H; C*H*=N), 7.29 (d, $^3J_{HH}$ = 7.7 Hz, 2H; NC$_6$*H*$_3$), 7.23 (t, $^3J_{HH}$ = 7.2 Hz, 1H; NC$_6$*H*$_3$), 7.16 (overlapping signals, 3H; NC$_6$*H*$_3$), 7.04 (d, $^3J_{HH}$ = 8.1 Hz, 1H; C$_6$*H*$_4$), 6.86 (t, $^3J_{HH}$ = 8.5 Hz, 1H; C$_6$*H*$_4$), 6.25 (overlapping m, 1H; C$_6$*H*$_4$ and 1H; C$_6$*H*$_4$), 3.43 (br m, 8H; OC*H*$_2$CH$_2$), 3.28 (m, 2H: C*H*(CH$_3$)$_2$), 3.09 (m, 2H; C*H*(CH$_3$)$_2$), 1.31 (m, 12H; CH(C*H*$_3$)$_2$), 1.25 (br m, 8H; OCH$_2$C*H*$_2$), 1.20 (d, $^3J_{HH}$ = 6.7 Hz, 6H; CH(C*H*$_3$)$_2$), 1.15 (d, $^3J_{HH}$ = 6.6 Hz, 6H; CH(C*H*$_3$)$_2$), 0.02 (s, 18H; CH(Si(C*H*$_3$)$_3$)$_2$), −1.84 ppm (s, 1H; C*H*(Si(CH$_3$)$_3$)$_2$); ^{13}C{^{1}H} NMR (C_6D_6, 298 K, 125.76 MHz): δ = 171.1 (*C*H=N), 159.3 (*i*-N=CH*C*$_6$H$_4$), 149.7 (*i*-N*C*$_6$H$_3$), 146.2 (*i*-N*C*$_6$H$_3$), 144.3 (*o*-N*C*$_6$H$_3$), 141.0 (*o*-N*C*$_6$H$_3$), 139.6 (*C*$_6$H$_4$), 134.0 (*C*$_6$H$_4$), 126.6 (*p*-N*C*$_6$H$_3$), 125.8 (*m*-N*C*$_6$H$_3$), 125.2 (*p*-N*C*$_6$H$_3$), 124.8 (*m*-N*C*$_6$H$_3$), 118.9 (*C*$_6$H$_4$), 117.5 (N*C*$_6$H$_4$), 111.7 (*C*$_6$H$_4$), 68.8 (O*C*H$_2$CH$_2$), 29.5 (*C*H(CH$_3$)$_2$), 28.9 (*C*H(CH$_3$)$_2$), 26.4 (CH(*C*H$_3$)$_2$), 26.2 (CH(*C*H$_3$)$_2$), 25.9 (CH(*C*H$_3$)$_2$), 25.8 (OCH$_2$*C*H$_2$), 23.7 (CH(*C*H$_3$)$_2$), 14.7 (*C*H(Si(CH$_3$)$_3$)$_2$), 6.4 ppm (CH(Si(*C*H$_3$)$_3$)$_2$); elemental analysis calcd (%) for $C_{46}H_{74}N_2O_2Si_2Sr$ (830.88 g mol^{-1}): C 66.49, H 8.98, N 3.37; found: C 66.52, H 8.92, N 3.38.

[{N^N}Ba{CH(SiMe$_3$)$_2$}(thf)$_2$] (10): Following a procedure similar to that described for **8**, the reaction of {N^N}H (0.39 g, 0.88 mmol) and $KCH(SiMe_3)_2$ (0.35 g, 1.77 mmol) with BaI_2 (0.35 g, 0.90 mmol) afforded **10** (0.41 g, 52%) as a yellow powder. Yellow crystals of **10** suitable for single-crystal X-ray crystallography were obtained by storage of a concentrated pentane solution at −30 °C. ^{1}H NMR (C_6D_6, 298 K, 500.13 MHz): δ = 8.06 (s, 1H; C*H*=N), 7.27 (d, $^3J_{HH}$ = 7.4 Hz, 2H; NC$_6$*H*$_3$), 7.18 (t, $^3J_{HH}$ = 6.6 Hz, 1H; NC$_6$*H*$_3$), 7.16 (overlapping signals, 3H; NC$_6$*H*$_3$), 7.10 (dd, $^3J_{HH}$ = 7.9 Hz, $^4J_{HH}$ = 1.8 Hz, 1H; C$_6$*H*$_4$), 6.91 (td, $^3J_{HH}$ = 7.7 Hz, $^4J_{HH}$ = 1.8 Hz, 1H; C$_6$*H*$_4$), 6.27 (td, $^3J_{HH}$ = 7.3 Hz, $^4J_{HH}$ = 1.1 Hz, 1H; C$_6$*H*$_4$), 6.19 (d, $^3J_{HH}$ = 8.8 Hz, 1H; C$_6$*H*$_4$), 3.43 (overlapping m, 8H; OC*H*$_2$CH$_2$ and 2H; C*H*(CH$_3$)$_2$), 3.12 (m, 2H; C*H*(CH$_3$)$_2$), 1.33 (d, $^3J_{HH}$ = 6.7 Hz, 6H; CH(C*H*$_3$)$_2$), 1.27 (overlapping m, 8H; OCH$_2$C*H*$_2$ and 6H; C*H*(CH$_3$)$_2$), 1.21 (d, $^3J_{HH}$ = 6.7 Hz, 6H; CH(C*H*$_3$)$_2$), 1.16 (d, $^3J_{HH}$ = 6.3 Hz, 6H; CH(C*H*$_3$)$_2$), 0.08 (s, 18H; CH(Si(C*H*$_3$)$_3$)$_2$), −1.78 ppm (s, 1H; C*H*(Si(CH$_3$)$_3$)$_2$); ^{13}C{^{1}H} NMR (C_6D_6, 298 K, 125.76 MHz): δ = 169.2 (*C*H=N), 157.8 (*i*-N=CH*C*$_6$H$_4$), 149.5 (*i*-N*C*$_6$H$_3$), 145.9 (*i*-N*C*$_6$H$_3$), 144.8 (*o*-N*C*$_6$H$_3$), 141.0 (*o*-N*C*$_6$H$_3$), 139.5 (*C*$_6$H$_4$), 134.3 (*C*$_6$H$_4$), 126.3 (*p*-N*C*$_6$H$_3$), 125.9 (*m*-N*C*$_6$H$_3$), 125.0 (*p*-N*C*$_6$H$_3$), 124.9 (*m*-N*C*$_6$H$_3$), 118.5 (*C*$_6$H$_4$), 111.5 (N*C*$_6$H$_4$), 111.4 (*C*$_6$H$_4$), 68.5 (O*C*H$_2$CH$_2$), 29.5 (*C*H(CH$_3$)$_2$), 28.8 (*C*H(CH$_3$)$_2$), 26.6 (CH(*C*H$_3$)$_2$), 26.2 (CH(*C*H$_3$)$_2$), 25.9 (CH(*C*H$_3$)$_2$), 25.7 (OCH$_2$*C*H$_2$), 23.8(CH(*C*H$_3$)$_2$), 14.7 (*C*H(Si(CH$_3$)$_3$)$_2$), 6.3 ppm (CH(Si(*C*H$_3$)$_3$)$_2$); elemental analysis calcd (%) for $C_{46}H_{74}N_2O_2Si_2Ba$ (880.55 g mol^{-1}): C 62.74, H 8.47, N 3.18; found: C 62.58, H 8.56, N 3.10.

NMR monitoring of cyclohydroamination reactions: In a glovebox, the catalyst was loaded into an NMR tube. The subsequent manipulations

were performed using standard Schlenk techniques. The substrate and solvent (C_6D_6, (0.6 or 1.2 mL as required) were then added to the NMR tube. The tube was sealed and vigorously shaken, then inserted into the probe of a Bruker AM 500 NMR spectrometer preheated to the required temperature. The reaction kinetics were monitored (using the multi zgvd command; D1 = 0.2 s; DS = 0; NS = 4 or more) over the course of 3 or more half-lives on the basis of amine consumption, by comparing the relative intensities of resonances diagnostic of substrate and product.

Typical protocol for intermolecular hydrofunctionalization reactions: In the glovebox, the catalyst (10 μmol) was loaded into an NMR tube. The subsequent manipulations were performed using standard Schlenk techniques. Styrene (58 μL, 500 μmol) and diphenylphosphine (87 μL, 500 μmol) were added to the NMR tube using microsyringes. The NMR tube was sealed and shaken vigorously, then put into an oil bath at 60 °C. The reaction times were measured from this point. After the required amount of time, the reaction was quenched and C_6D_6 was added to the mixture at room temperature. The conversion was determined according to the ^{1}H NMR spectrum of the reaction mixture.

X-ray diffraction crystallography: Suitable crystals for X-ray diffraction analysis of **2′**, **4**–**5**, **7**, **9**·C_5H_{12}, and **10** were obtained by recrystallization of the purified compounds. Diffraction data were collected at 150(2) K using a Bruker APEX CCD diffractometer with graphite-monochromated $Mo_{K\alpha}$ radiation ($\lambda = 0.71073$ Å). A combination of ω and Φ scans was carried out to obtain at least a unique data set. The crystal structures were solved by direct methods, remaining atoms were located from difference Fourier synthesis followed by full-matrix least-squares refinement based on F2 (programs SIR97 and SHELXL-97).[59] Many hydrogen atoms could be found from the Fourier difference analysis. Carbon- and oxygen-bound hydrogen atoms were placed at calculated positions and forced to ride on the attached atom. The hydrogen atom contributions were calculated but not refined. All non-hydrogen atoms were refined with anisotropic displacement parameters. The locations of the largest signals in the final difference Fourier map calculation as well as the magnitude of the residual electron densities were of no chemical significance. Relevant collection and refinement data are summarized in the Supporting Information (S42).[60]

CCDC-918568 (**2′**), -918569 (**4**), -918570 (**5**), -918571 (**7**), -918572 (**9**)·C_5H_{12}, -918573 (**10**), contain the supplementary crystallographic data for this paper. These data can be obtained free of charge from The Cambridge Crystallographic Data Centre via www.ccdc.cam.ac.uk/data_request/cif.

Acknowledgements

We thank the European Research Council (grant FP7-People-2010-IIF *ChemCatSusDe*), the CNRS and the University of Rennes 1 for financial support. The assistance of Stephen Boyer (London Metropolitan University) with elemental analyses and Dr. Vincent Dorcet (*Institut des Sciences Chimiques de Rennes*) with the X-ray structure of complex **7** is also gratefully acknowledged.

[1] *Catalytic Heterofunctionalization: from Hydroamination to Hydrozirconation* (Eds.: A. Togni, H. Grützmacher), Wiley-VCH, Weinheim, **2001**.

[2] For leading reviews: a) K. C. Hultzsch, *Adv. Synth. Catal.* **2005**, *347*, 367; b) D. S. Glueck, *Chem. Eur. J.* **2008**, *14*, 7108; c) T. E. Müllller, K. C. Hultzsch, M. Yus, F. Foubelo, M. Tada, *Chem. Rev.* **2008**, *108*, 3795; d) D. S. Glueck, *Top. Organomet. Chem.* **2010**, *31*, 65.

[3] S. Hong, T. J. Marks, *Acc. Chem. Res.* **2004**, *37*, 673 and references cited therein.

[4] For the alkali-mediated hydroamination of alkenes: J. Seayad, A. Tillack, C. G. Hartung, M. Beller, *Adv. Synth. Catal.* **2002**, *344*, 795 and references therein.

[5] For the (cyclo)hydrophosphination of alkenes with late transition metals: a) P. G. Pringle, M. B. Smith, *J. Chem. Soc. Chem. Commun.* **1990**, 1701; b) D. K. Wicht, I. V. Kourkine, B. M. Lew, J. Mulei Nthenge, D. S. Glueck, *J. Am. Chem. Soc.* **1997**, *119*, 5039; c) D. K. Wicht, I. V. Kourkine, I. Kovacik, D. S. Glueck, *Organometallics* **1999**, *18*, 5381; d) M. O. Shulyupin, M. A. Kazankova, I. P. Beletskaya, *Org. Lett.* **2002**, *4*, 761.

[6] For a case of titanium-catalyzed 1,4-hydrophosphination of 1,3-dienes: A. Perrier, V. Comte, C. Moïse, P. Le Gendre, *Chem. Eur. J.* **2010**, *16*, 64.

[7] a) M. R. Douglass, T. J. Marks, *J. Am. Chem. Soc.* **2000**, *122*, 1824; b) M. R. Douglass, C. L. Stern, T. J. Marks, *J. Am. Chem. Soc.* **2001**, *123*, 10221; c) M. R. Douglass, M. Ogasawara, S. Hong, M. V. Metz, T. J. Marks, *Organometallics* **2002**, *21*, 283.

[8] Cyclohydroamination of aminoalkenes: a) M. R. Gagné, T. J. Marks, *J. Am. Chem. Soc.* **1989**, *111*, 4108; b) M. R. Gagné, S. P. Nolan, T. J. Marks, *Organometallics* **1990**, *9*, 1716; c) M. R. Gagné, T. J. Marks, *J. Am. Chem. Soc.* **1992**, *114*, 275; d) M. A. Giardello, V. P. Conticello, L. Brard, M. R. Gagné, T. J. Marks, *J. Am. Chem. Soc.* **1994**, *116*, 10241; e) J.-S. Ryu, T. J. Marks, F. E. McDonald, *Org. Lett.* **2001**, ***3***, 3091.

[9] Intermolecular hydroamination of alkenes: a) Y. Li, T. J. Marks, *Organometallics* **1996**, *15*, 3770; b) J.-S. Ryu, G. Y. Li, T. J. Marks, *J. Am. Chem. Soc.* **2003**, *125*, 12584.

[10] For reviews, see references [2a], [2c] and: a) I. Aillaud, J. Collin, J. Hannedouche, E. Schulz, *Dalton Trans.* **2007**, 5105; b) J. Hannedouche, J. Collin, A. Trifonov, E. Schulz, *J. Organomet. Chem.* **2011**, *696*, 255. For key contributions, see: c) P. J. Walsh, A. M. Baranger, R. G. Bergman, *J. Am. Chem. Soc.* **1992**, *114*, 1708; d) P. L. McGrane, M. Jensen, T. Livinghouse, *J. Am. Chem. Soc.* **1992**, *114*, 5459; e) E. Haak, I. Bytschkov, S. Doye, *Angew. Chem.* **1999**, *111*, 3584; *Angew. Chem. Int. Ed.* **1999**, *38*, 3389; f) C. Li, R. K. Thomson, B. Gillon, B. O. Patrick, L. L. Schafer, *Chem. Commun.* **2003**, 2462; g) L. Ackermann, R. G. Bergman, R. N. Loy, *J. Am. Chem. Soc.* **2003**, *125*, 11956; h) J. Collin, J.-C. Daran, E. Schulz, A. A. Trifonov, *Chem. Commun.* **2003**, 3048; i) P. D. Knight, I. Munslow, P. N. O'Shaughnessy, P. Scott, *Chem. Commun.* **2004**, 894; j) D. V. Gribkov, K. C. Hultzsch, *Angew. Chem.* **2004**, *116*, 5659; *Angew. Chem. Int. Ed.* **2004**, *43*, 5542; k) J. Collin, J.-C. Daran, O. Jacquet, E. Schulz, A. A. Trifonov, *Chem. Eur. J.* **2005**, *11*, 3455; l) D. V. Gribkov, K. C. Hultzsch, F. Hampel, *J. Am. Chem. Soc.* **2006**, *128*, 3748; m) M. C. Wood, D. C. Leitch, C. S. Yeung, J. A. Kozak, L. L. Schafer, *Angew. Chem.* **2006**, *119*, 358; *Angew. Chem. Int. Ed.* **2006**, *46*, 354; n) A. L. Gott, A. J. Clarke, G. J. Clarkson, P. Scott, *Chem. Commun.* **2008**, 1422; o) I. Aillaud, J. Collin, C. Duhayon, R. Guillot, D. Lyubov, E. Schulz, A. A. Trifonov, *Chem. Eur. J.* **2008**, *14*, 2189; p) J. Hannedouche, I. Aillaud, J. Collin, E. Schulz, A. A. Trifonov, *Chem. Commun.* **2008**, 3552; q) A. V. Pawlikowski, A. Ellern, A. D. Sadow, *Inorg. Chem.* **2009**, *48*, 8020; r) L. E. N. Allan, G. J. Clarkson, D. J. Fox, A. L. Gott, P. Scott, *J. Am. Chem. Soc.* **2010**, *132*, 15308; s) A. L. Reznichenko, H. N. Nguyen, K. C. Hultzsch, *Angew. Chem.* **2010**, *122*, 9168; *Angew. Chem. Int. Ed.* **2010**, *49*, 8984; t) D. C. Leitch, R. H. Platel, L. L. Schafer, *J. Am. Chem. Soc.* **2011**, *133*, 15453; u) K. Manna, S. Xu, A. D. Sadow, *Angew. Chem.* **2011**, *123*, 1905; *Angew. Chem. Int. Ed.* **2011**, *50*, 1865; v) A. L. Reznichenko, K. C. Hultzsch, *Organometallics* **2013**, *32*, 1394; w) J. Hannedouche, E. Schulz, *Chem. Eur. J.* **2013**, *19*, 4972.

[11] a) M. R. Crimmin, I. J. Casely, M. S. Hill, *J. Am. Chem. Soc.* **2005**, *127*, 2042; b) A. G. M. Barrett, M. R. Crimmin, M. S. Hill, P. B. Hitchcock, G. Kociok-Köhn, P. A. Procopiou, *Inorg. Chem.* **2008**, *47*, 7366; c) A. G. M. Barrett, I. J. Casely, M. R. Crimmin, M. S. Hill, J. R. Lachs, M. F. Mahon, P. A. Procopiou, *Inorg. Chem.* **2009**, *48*, 4445; d) M. R. Crimmin, M. Arrowsmith, A. G. M. Barrett, I. J. Casely, M. S. Hill, P. A. Procopiou, *J. Am. Chem. Soc.* **2009**, *131*, 9670; e) M. Arrowsmith, M. S. Hill, G. Kociok-Köhn, *Organometallics* **2009**, *28*, 1730; f) M. Arrowsmith, M. S. Hill, G. Kociok-Köhn, *Organometallics* **2011**, *30*, 1291; g) M. Arrowsmith, M. R. Crimmin, A. G. M. Barrett, M. S. Hill, G. Kociok-Köhn, P. A. Procopiou, *Organometallics* **2011**, *30*, 1493.

[12] a) A. G. M. Barrett, C. Brinkmann, M. R. Crimmin, M. S. Hill, P. Hunt, P. A. Procopiou, *J. Am. Chem. Soc.* **2009**, *131*, 12906; b) C.

Brinkmann, A. G. M. Barrett, M. S. Hill, P. A. Procopiou, *J. Am. Chem. Soc.* **2012**, *134*, 2193.

[13] M. R. Crimmin, A. G. M. Barrett, M. S. Hill, P. B. Hitchcock, P. A. Procopiou, *Organometallics* **2007**, *26*, 2953.

[14] a) M. R. Crimmin, A. G. M. Barrett, M. S. Hill, P. A. Procopiou, *Org. Lett.* **2007**, *9*, 331; b) A. G. M. Barrett, T. C. Boorman, M. R. Crimmin, M. S. Hill, G. Kociok-Köhn, P. A. Procopiou, *Chem. Commun.* **2008**, 5206; c) J. R. Lachs, A. G. M. Barrett, M. R. Crimmin, G. Kociok-Köhn, M. S. Hill, M. F. Mahon, P. A. Procopiou, *Eur. J. Inorg. Chem.* **2008**, 4173; d) M. R. Crimmin, A. G. M. Barrett, M. S. Hill, P. B. Hitchcock, P. A. Procopiou, *Organometallics* **2008**, *27*, 497; e) C. Brinkmann, A. G. M. Barrett, M. S. Hill, P. A. Procopiou, S. Reid, *Organometallics* **2012**, *31*, 7287.

[15] M. H. Chisholm, J. Gallucci, K. Phomphrai, *Chem. Commun.* **2003**, 48.

[16] a) S. Datta, P. W. Roesky, S. Blechert, *Organometallics* **2007**, *26*, 4392; b) S. Datta, M. T. Gamer, P. W. Roesky, *Organometallics* **2008**, *27*, 1207; c) F. Buch, S. Harder, *Z. Naturforsch. B* **2008**, *63*, 169; d) J. Jenter, R. Köppe, P. W. Roesky, *Organometallics* **2011**, *30*, 1404; e) J. S. Wixey, B. D. Ward, *Chem. Commun.* **2011**, *47*, 5449; f) J. S. Wixey, B. D. Ward, *Dalton Trans.* **2011**, *40*, 7693; g) T. D. Nixon, B. D. Ward, *Chem. Commun.* **2012**, *48*, 11790.

[17] H. Hu, C. Cui, *Organometallics* **2012**, *31*, 1208.

[18] For the Ca-mediated hydrophosphination of alkynes, see: a) T. M. A. Al-Shboul, H. Görls, M. Westerhausen, *Inorg. Chem. Commun.* **2008**, *11*, 1419; b) T. M. A. Al-Shboul, V. K. Pálfi, L. Yu, R. Kretschmer, K. Wimmer, R. Fischer, H. Görls, M. Reiher, M. Westerhausen, *J. Organomet. Chem.* **2011**, *696*, 216.

[19] Zinc and magnesium also yield efficient catalysts for the cyclohydroamination of aminoalkenes. For Zn, see: a) A. Zulys, M. Dochnahl, D. Hollmann, K. Löhnwitz, J.-S. Herrmann, P. W. Roesky, S. Blechert, *Angew. Chem.* **2005**, *117*, 7972; *Angew. Chem. Int. Ed.* **2005**, *44*, 7794; b) M. Dochnahl, J.-W. Pissarek, S. Blechert, K. Löhnwitz, P. W. Roesky, *Chem. Commun.* **2006**, 3405; c) M. Dochnahl, K. Löhnwitz, J.-W. Pissarek, M. Biyikal, S. R. Schulz, S. Schön, N. Meyer, P. W. Roesky, S. Blechert, *Chem. Eur. J.* **2007**, *13*, 6654; d) A. Mukherjee, T. K. Sen, P. K. Ghorai, P. P. Samuel, C. Schulzke, S. K. Mandal, *Chem. Eur. J.* **2012**, *18*, 10530. For Mg, see: e) X. Zhang, T. J. Emge, K. C. Hultzsch, *Organometallics* **2010**, *29*, 5871; f) J. F. Dunne, D. Bruce Fulton, A. Ellern, A. D. Sadow, *J. Am. Chem. Soc.* **2010**, *132*, 17680; g) S. Tobisch, *Chem. Eur. J.* **2011**, *17*, 14974; h) T. J. Emge, K. C. Hultzsch, *Angew. Chem.* **2012**, *124*, 406; *Angew. Chem. Int. Ed.* **2012**, *51*, 394.

[20] B. Liu, T. Roisnel, J.-F. Carpentier, Y. Sarazin, *Angew. Chem. Int. Ed.* **2012**, *51*, 4943.

[21] B. Liu, T. Roisnel, J.-F. Carpentier, Y. Sarazin, *Chem. Eur. J.* **2013**, *19*, 2784.

[22] R. D. Shannon, *Acta Crystallogr.* **1976**, *A32*, 751.

[23] a) S. Harder, *Angew. Chem.* **2004**, *116*, 2768; *Angew. Chem. Int. Ed.* **2004**, *43*, 2714; b) T. K. Panda, A. Zulys, M. T. Gamer, P. W. Roesky, *J. Organomet. Chem.* **2005**, *690*, 5078; c) B. Liu, T. Roisnel, L. Maron, J.-F. Carpentier, Y. Sarazin, *Chem. Eur. J.* **2013**, *19*, 3986.

[24] K. Takaki, G. Koshoji, K. Komeyama, M. Takeda, T. Shishido, A. Kitani, K. Takehira, *J. Org. Chem.* **2003**, *68*, 6554.

[25] P. G. Hayes, G. C. Welch, D. J. H. Emslie, C. L. Noack, W. E. Piers, M. Parvez, *Organometallics* **2003**, *22*, 1577.

[26] C. Ruspic, J. Spielmann, S. Harder, *Inorg. Chem.* **2007**, *46*, 5320.

[27] The X-ray structure of $[\{N\hat{}N\}_2Sm^{II}(thf)]$ is given in the supporting information.

[28] See the supporting information for details.

[29] a) S. C. Sockwell, T. P. Hanusa, J. C. Huffman, *J. Am. Chem. Soc.* **1992**, *114*, 3393; b) D. F.-J. Piesik, K. Häbe, S. Harder, *Eur. J. Inorg. Chem.* **2007**, 5652; c) M. R. Crimmin, A. G. M. Barrett, M. S. Hill, D. J. MacDougall, M. F. Mahon, P. A. Procopiou, *Dalton Trans.* **2009**, 9715.

[30] a) A. Weeber, S. Harder, H. H. Brintzinger, K. Knoll, *Organometallics* **2000**, *19*, 1325; b) F. Feil, S. Harder, *Eur. J. Inorg. Chem.* **2003**, 3401.

[31] Note however that upon attempts to prepare Ae-hydride complexes by reaction of $[\{N\hat{}N\}Ae\{N(SiMe_3)_2\}(thf)_n]$ (**1**–**3**) with $PhSiH_3$, unexpected reduction and reactivity of the iminoanilide ligand were observed, repeatedly leading to 1,3-bis(2,6-diisopropylphenyl)-2-phenyl-1,2,3,4-tetrahydrobenzo[*d*][1,3,2]diazasiline, which has been fully characterized by NMR and X-ray diffraction techniques, see the supporting information for details. This compound is structurally similar to the product of the reaction of a divalent silylene and C_6F_5H as described by Roesy et al.: A. Jana, P. P. Samuel, G. Tavčar, H. W. Roesky, C. Schulzke, *J. Am. Chem. Soc.* **2010**, *132*, 10164.

[32] Only 15 entries were found for 4-coordinate Sr complexes in the CCDC database at the time of writing, and amongst these only 2 were heteroleptic compounds of the type $[\{L\}Sr(X)(solvent)_n]$.

[33] S. Sarish, S. Nembenna, S. Nagendran, H. W. Roesky, A. Pal, R. Herbst-Irmer, A. Ringe, J. Magull, *Inorg. Chem.* **2008**, *47*, 5971.

[34] A. W. Addison, T. N. Rao, J. Reedijk, J. van Rijn, G. C. Verschoor, *J. Chem. Soc. Dalton Trans.* **1984**, 1349.

[35] R. Jiao, X. Shen, M. Xue, Y. Zhang, Y. Yao, Q. Shen, *Chem. Commun.* **2010**, *46*, 4118.

[36] Sr complexes with σ-bound alkyl groups that have been structurally characterized include: $[Sr([18]crown\text{-}6)(C{\equiv}CSiPh_3)_2]$ (Sr–C = 2.69, 2.72 Å) and $[Sr([18]crown\text{-}6)(C{\equiv}C\text{-}C_6H_4\text{-}p\text{-}tBu)_2]$ (Sr–C = 2.68 Å), the bis-alkyl $[Sr\{CH(SiMe_3)_2\}_2(thf)_3]$ (Sr-C = 2.68, 2.69 Å), $[\{(BDI)Sr(C{\equiv}CPh)(thf)\}_2]$ (Sr–C = 2.69 Å), $[\{(Me_3Si)_2(MeOMe_2Si)\text{-}C\}_2Sr(thf)]$ (Sr–C = 2.79, 2.85 Å), $[(2\text{-}Me_2N\text{-}\alpha\text{-}Me_3Si\text{-}benzyl)_2Sr(thf)_2]$ (Sr-C = 2.77, 2.80 Å), or $[\{(thf)_2Sr\{CH(SiMe_3)_2\}(\mu\text{-}BH_3NH_2)\}_2]$ (Sr-C = 2.69 Å). See: a) D. C. Green, U. Englich, K. Ruhlandt-Senge, *Angew. Chem.* **1999**, *111*, 365; *Angew. Chem. Int. Ed.* **1999**, *38*, 354; b) M. A. Guino-o, J. S. Alexander, M. L. McKee, H. Hope, U. B. Englich, K. Ruhlandt-Senge, *Chem. Eur. J.* **2009**, *15*, 11842; c) M. R. Crimmin, A. G. M. Barrett, M. S. Hill, D. J. MacDougall, M. F. Mahon, P. A. Procopiou, *Chem. Eur. J.* **2008**, *14*, 11292; d) A. Stasch, S. P. Sarish, H. W. Roesky, K. Meindl, F. Dall′Antonia, T. Schulz, D. Stalke, *Chem. Asian J.* **2009**, *4*, 1451; e) K. Izod, S. T. Liddle, W. Clegg, *J. Am. Chem. Soc.* **2003**, *125*, 7534; f) F. Feil, S. Harder, *Organometallics* **2001**, *20*, 4616; g) P. Bellham, M. S. Hill, D. J. Liptrot, D. J. MacDougall, M. F. Mahon, *Chem. Commun.* **2011**, *47*, 9060.

[37] A search on the CCDC database for compounds incorporating Ba–C bonds gave 33 hits.

[38] Structurally characterized heteroleptic $[\{L\}BaX(solvent)_n]$ (X = aryl, amide, halide) featuring Ba–C bonds are restricted to the dimeric bis(phosphinimino)methanide complex $[(\{(Me_3SiNPPh_2)_2CH\}BaI(thf)_2)_2]$, the tris(imidazolin-2-ylidene-1-yl)borate complex $[\{HB(ImtBu)_3\}Ba\{N(SiMe_3)_2\}(thf)](ImtBu)_{1.5}]$ (ImtBu = N-*tert*-butyl-imidazole) and a highly congested pentafluorophenyl triazenide complex $[\{N_3ArAr'\}Ba(C_6F_5)]$ where Ar and Ar′ are bulky aryl substituents. See reference [23b] and: a) S.-O. Hauber, F. Lissner, G. B. Deacon, M. Niemeyer, *Angew. Chem.* **2005**, *117*, 6021; *Angew. Chem. Int. Ed.* **2005**, *44*, 5871; b) M. Arrowsmith, A. Heath, M. S. Hill, P. B. Hitchcock, G. Kociok-Köhn, *Organometallics* **2009**, *28*, 4550.

[39] A. G. Avent, M. R. Crimmin, M. S. Hill, P. B. Hitchcock, *Dalton Trans.* **2005**, 278.

[40] This difference can perhaps be linked to the presence of the fully occupied inner f orbitals ($4f^{14}$) in the case of **7**, yet electronic repulsions based of filled f orbitals in **7** would probably also have consequences on other metric parameters in this complex.

[41] B. Liu, V. Dorcet, L. Maron, J.-F. Carpentier, Y. Sarazin, *Eur. J. Inorg. Chem.* **2012**, 3023.

[42] K. C. Hultzsch, F. Hampel, T. Wagner, *Organometallics* **2004**, *23*, 2601.

[43] pK_a $(CH_2(SiMe_3)_2/CH(SiMe_3)_2^-) > 40$; pK_a $(HN(SiMe_3)_2/N(SiMe_3)_2^-) = 25.8$.

[44] R. K. Thomson, J. A. Bexrud, L. L. Schafer, *Organometallics* **2006**, *25*, 4069.

[45] Investigations with higher amine and styrene loadings for long reaction times (60–120 min) could not be performed with **10** in the way it was done for **3** due to the ability of the former to promote the

polymerization of styrene, even at room temperature. For the Ae-catalyzed polymerization of styrene, see reference [23a].

[46] A. G. Trambitas, D. Melcher, L. Hartenstein, P. W. Roesky, C. Daniliuc, P. G. Jones, M. Tamm, *Inorg. Chem.* **2012**, *51*, 6753.

[47] Such study is beyond the scope of this manuscript and will be the topic of a later report.

[48] These data are purely qualitative and aimed at giving a brief overview of the influence of the *para* substituent on reaction rates. A quantitative Hammett investigation could not be carried out owing to experimental constraints. The observed trend $CF_3 > Cl > H > Me > t\text{Bu} > OMe$ is compatible with the proposed mechanism. Yet caution must be paid in the global interpretation of these data as more than one step involves styrenics in this scenario, including binding to the metal center which should be disfavored by electron-withdrawing *p*-substituents.

[49] Reaction conditions: $T = 60\,^{\circ}C$, solvent C_6D_6, $[\text{precatalyst}]_0/[\text{styrene}]_0/[HPPh_2]_0 = 1:80:8$, precatalyst: 10.0 μmol, total volume C_6D_6 + styrene + $HPPh_2$ = 0.6 mL.

[50] The studies could not be extended to the paramagnetic **5**, nor to the alkyl complexes **9**–**10** which catalyzed these reactions too rapidly for accurate measurements.

[51] The activation energy determined for the hydrophosphination of *p*-Cl-styrene catalyzed by **3**, $E_a = 24.1(1.3)\ kJ\,mol^{-1}$, was smaller than that determined for styrene under identical conditions ($E_a = 34.2(2.4)\ kJ\,mol^{-1}$, Table 6, entry 3). Reactions with *p*-Me-styrene in C_6D_6 were too slow to be monitored below 80 °C, but the following values of k_{app} were determined: 1.37×10^{-4} (*p*-Me-styrene, 80 °C), 9.51×10^{-4} (styrene, 70 °C) and $11.27 \times 10^{-4}\ s^{-1}$ (*p*-Cl-styrene, 70 °C). Apart from the temperature, all other parameters remained identical between the three experiments, which therefore further supported the reactivity trend Cl > H > Me in *para*-substituted styrene derivatives.

[52] J.-N. Li, L. Liu, Y. Fu, Q.-X. Guo, *Tetrahedron* **2006**, *62*, 4453 and references therein.

[53] J. Eppinger, M. Spiegler, W. Hieringer, W. A. Herrmann, R. Anwander, *J. Am. Chem. Soc.* **2000**, *122*, 3080.

[54] The superiority of Ae-alkyl catalysts (**8**–**10**) over Ae-amide (**1**–**3**) in intermolecular hydrophosphination is less pronounced than seen in hydroamination reactions. This is mostly due to the higher acidity of phosphines with respect to amines/aminoalkenes. The protonolysis of the Ae-amide bond in **1**–**3** will be shifted more towards the formation of the catalytically active species with $HPPh_2$ than with an amine (Scheme 2 and 4), whereas the difference between the two substrates will not be obvious with the very basic Ae-alkyl **8**–**10**. Consistent with this, the ^1H NMR monitoring of the hydrophosphination of styrene derivatives with $HPPh_2$ catalyzed by **3** and **10** indicated quantitative release of $HN(SiMe_3)_2$ and $CH_2(SiMe_3)_2$, respectively.

[55] The lanthanide-catalyzed cyclohydrophosphination of phosphinoalkenes proceeded with the following rate-law: $R_{CHP} = k[\text{substrate}]^0[\text{precatalyst}]^1$, see reference [7].

[56] B. Liu, J.-F. Carpentier, Y. Sarazin, *Chem. Eur. J.* **2012**, *18*, 13259.

[57] P. Girard, J. L. Namy, H. B. Kagan, *J. Am. Chem. Soc.* **1980**, *102*, 2693.

[58] F. G. N. Cloke, P. B. Hitchcock, M. F. Lappert, G. A. Lawless, B. Royo, *J. Chem. Soc. Chem. Commun.* **1991**, 724.

[59] a) G. M. Sheldrick, SHELXS-97, Program for the Determination of Crystal Structures; University of Goettingen: Germany, **1997**; b) G. M. Sheldrick, SHELXL-97, Program for the Refinement of Crystal Structures; University of Göttingen, Göttingen (Germany), **1997**.

[60] CIF files containing complete crystallographic data for all reported crystal structures, figures of X-ray structures of additional compounds, summary of crystallographic data for complexes **2′**, **4**, **5**, **7**, **9**·C_5H_{12}, and **10**, detailed kinetic data for hydroelementation reactions, NMR data for isolated new tertiary phosphines are contained in the Supporting Information (32 pages).

Received: April 17, 2013
Published online: August 19, 2013

